Covert Transaction for Cognitive Integrated Satellite Aerial Ground Networks With NOMA and Imperfect Limitations

Liuying Zhou, Peilin Qi, *Graduate Student Member, IEEE*, Kefeng Guo, Ali Nauman, Lei Zhang, Qihui Wu, and Sung Won Kim

***Abstract*— Covert transaction (CT) is a popular topic investigated in recent years. In this research, we study the CT of the integrated satellite aerial ground networks (ISAGNs). Particularly, to optimize spectrum efficiency and resource utilization, cognitive technology and the non-orthogonal multiple access (NOMA) scheme are employed in the ISAGNs to improve the system's covert performance. Besides, to reflect real-world scenarios, the imperfect hardware, imperfect channel estimation, and the co-channel interferences are also investigated for the ISAGNs. Moreover, to reduce system complexity, the decode-and-forward scheme is implemented in the aerial relay to transmit the covert signal. In addition, a newly defined detection error probability (DEP) is proposed for the CT of the system under consideration. Furthermore, by taking these factors into account, the closed-form expressions for the DEP, outage probability (OP), and covert transmission rate (CTR) are also obtained. Finally, several representative Monte Carlo simulations are conducted to evaluate the impacts of system and channel parameters on the covert system performance.**

***Index Terms*— Covert transmission, integrated satellite aerial ground networks, cognitive technology, non-orthogonal multiple access, imperfect limitations, covert system performance.**

I. Introduction

IT HAS become the common view that the 5G and the next generation wireless networks are all coming, which leads us to the new wireless communication networks (NWCNs) [1], [2]. This NWCN has some characteristics such as wide coverage, high resource utilization efficiency, high system security, and so on [3]. To satisfy these requirements, some new techniques have come to our attention. Among these techniques, cognitive technology, non-orthogonal multiple access (NOMA), and covert transaction (CT) are the famous ones these years [4]. CT technology and NOMA techniques represent effective approaches for enhancing resource utilization efficiency, a prominent research focus in recent years. For the wide coverage, the integrated satellite aerial ground network (ISAGN) is considered as the preferred method that can satisfy the demand of wide coverage for the NWCNs [5], which has attracted so many researchers [6], [7]. The ISAGN has combined the advantages of satellite communications (SatComs), the ground communications (GCs), and the aerial communications (ACs), which have played an important role both in academic areas and industrial areas [8]. In academic areas, the ISAGN has been investigated by some people [9]. Within industrial sectors, ISAGN serves as a critical element of China's Integrated Space Ground Information Networks and constitutes a primary building block of Digital Video Broadcasting-Satellite (DVB-S) systems [10], [11].

A. Related Works

Due to the increasing power of satellite techniques, the ISAGN has emerged as a prevalent area of study in recent times [12]. In the research of ISAGN, the channel model holds paramount significance, particularly within the domain of SatCom. Numerous scholars have explored the model of the satellite channel and proposed some famous models that are fit for different cases, such as Rician channel model, Nakagami-*m* channel model, and Shadowed-Rician (SR) channel model. In these channel models, the SR channel model is the very famous one which has been used, for it has both the characteristics of Rician channel model and Nakagami-*m* channel model [13]. Some researchers have investigated the SR channel model in these years, such as Arti and Bhatnagar and Hjorungnes have used SR channel model to investigate the system performance for the ISAGN [14], [15]. Some researchers also investigated the ISAGN, for example, Min Lin and Kang An are the researchers who investigated this topic very early. The ISAGN's performance metrics, including ergodic capacity, outage probability, and symbol error ratio, were analyzed utilizing the SR model, unfortunately, the SR model they used consisted of special functions which was difficult to follow. Based on this foundation, Liang Yang proposed a general SR channel model, in which finite series were used. The investigations have become easier by applying

Received 9 September 2025; revised 12 October 2025; accepted 26 October 2025. Date of publication 3 November 2025; date of current version 8 December 2025. This work was supported in part by the Open Project Funds for the Joint Laboratory of Spatial Intelligent Perception and Large Model Application under Grant SIPLMA-2024-YB-02, and in part by the National Science Foundation of China under Grant 62001517. *(Corresponding authors: Kefeng Guo; Ali Nauman.)*

Liuying Zhou is with the School of Foreign Language, Yancheng Institute of Technology, Yancheng 224051, China (e-mail: linda7575@ycit.edu.cn).

Peilin Qi, Kefeng Guo, Lei Zhang, and Qihui Wu are with the College of Electronic and Information Engineering, Nanjing University of Aeronautics and Astronautics, Nanjing 210016, China (e-mail: peilin_qi@nuaa.edu.cn; guokefeng.cool@163.com; Zhang_lei@nuaa.edu.cn; wuqihui2014@sina.com).

Ali Nauman and Sung Won Kim are with the School of Computer Science and Engineering, Yeungnam University Republic of Korea, Gyeongsan 38541, Republic of Korea (e-mail: anauman@ynu.ac.kr; swon@yu.ac.kr).

Digital Object Identifier 10.1109/TCE.2025.3628386

this SR channel model, especially for some performance analysis work. On this foundation, Yang proposed a more popular SR channel model for the multiple antennas systems and multiple relays systems. In [16], a newly framework based on the ISAGN, incorporating LEO satellite constellations was proposed. In [17], the outage probability (OP) was investigated for the ISAGN by utilizing this SR channel model with multiple relays and multiple users. In [18], the OP of the uplink ISAGN featuring multiple terrestrial relays was analyzed using the proposed SR channel model. In [19], the ergodic capacity and OP were studied for the ISAGN by using these SR channel models. Besides the performance analysis works, the optimization works are also hot topics by using this SR channel model. In [20] and [21], the system metrics were optimized for the ISAGN by using this SR channel model. Several optimization methods were provided to enhance system performance.

From the former discussions, it can be known that high resource utilization efficiency is the basic requirement of the NWCNs. Thus, improving the resource utilization efficiency is the target requirement for the investigators. Building on this foundation, non-orthogonal multiple access (NOMA) and cognitive radio techniques are considered efficient solutions to address such requirements [22]. The investigations for the NOMA and cognitive technology are the hot topics these years, there are so many researchers following this topic, especially for the researchers in ISAGN. In [23], the authors investigated the cognitive technique for the ISAGN along with the closed expressions of the OP. In [24], the secure performance of the cognitive ISAGN was analyzed by deriving its closed-form expression. In [25], the secrecy performance of the ISAGN was enhanced with the aid of cognitive technique. In [26], the authors explored the power control strategy within the CISAGN framework. In [27], the secrecy capacity was optimized for the CISAGN through a robust secrecy-energy efficient beamforming technology. As announced before, the NOMA strategy is also considered as the wishing method to enhance the resource energy utilization efficiency, especially for the spectrum resource. This method enables simultaneous transmission of distinct signals within identical time slots via a single frequency band. To distinguish between signals, successive interference cancellation (SIC) is applied by decoding each according to its power level [28]. Lots of researchers have explored the NOMA scheme in wireless communication networks, especially in the ISAGNs. In [29], the investigators studied the ISAGN's OP characteristics by employing the NOMA strategy with imperfect channel state information (CSI). In [30], the authors investigated the impact of NOMA-based methods for the CISAGN with an active reconfigurable intelligent surface (RIS). In [31], the NOMA and orthogonal multiple access (OMA) mode was selected for the ISAGN with a resource allocation scheme. In [32], the symbol error ratio of the ISAGN was examined under the presence of the NOMA strategy.

Because the wireless channel changes rapidly, acquiring accurate CSI is challenging, which introduces imperfections into the channel model [33]. To address this issue, channel estimation is necessary to obtain precise CSI of the transmission channel. Nevertheless, it is important to note that channel estimation errors (CEEs) frequently occur in wireless systems, particularly in ISAGNs, due to the intrinsic properties of satellite channel models. In [34], the impact of CEE on SatCom was examined. In [35], the impact of CEE was investigated for the ISAGN with the cognitive technique and NOMA strategy. As discussed before, the wide coverage is an inherent demand for the NWCNs. Owing to wireless broadcast nature and the wide coverage of satellite-enabled Internet of Things (IoT) networks, IoT devices are vulnerable to being targeted by eavesdropping attempts. However, owing to the same reasons, the security problem has become the facing serious problem that should be solved for the NWCNs [36]. As mentioned before, the ISAGN is the major part of the NWCNs, thus the security problem is also a major challenge for the ISAGNs [37]. For addressing secrecy challenges in NWCNs as well as ISAGNs, physical layer security (PLS) is viewed as a desirable approach [38]. In [39], the authors reviewed all the secrecy challenges of ISAGNs and proposed several research directions for future studies. In [40], a threshold-based selection scheme was put forward by the authors for ISAGNs involving multiple legitimate users and eavesdroppers, while analyzing the system's secrecy outage probability (SOP) and average secrecy capacity (ASC). In [41], the security issue was optimized for the ISAGNs with several optimization methods. It is worth noting that security issues are also present in ISAGNs employing the NOMA scheme [42], [43], [44], [45]. In [42], a robust security protocol for NOMA-based ISAGNs was formulated by the authors. In [43], the authors assessed how ISAGNs perform in terms of secrecy when the NOMA technique is combined with simultaneous wireless information and power transfer. In [44], an anti-jamming transmission scheme is developed for the secrecy performance of the NOMA-based ISAGNs. Through [45], the authors proposed some secrecy research directions for the ISAGNs in the presence of NOMA scheme. However, in practical systems, a better method to gain the system security is proactive eavesdropping, which transmits an artificial noise or the jamming signals to found an active CT, which can affect the warden's detection [46], [47]. The CT has become a hot topic in ISAGNs, and many researchers have investigated this topic. In [48], the CT was examined for the ISAGN using an opportunistic scheduling strategy and cooperative jamming. In [49], the authors investigated the CT in ISAGNs featuring multiple Low Earth Orbit (LEO) satellites. In [50], the CT was studied in the RIS-aided ISAGNs. In [51], the CT was investigated in Intelligent Transportation Systems(ITS).

B. Motivations

In practical systems, transmission nodes in wireless communication networks often experience imperfect hardware (IPH) [52], [53], [54]. In [55], the authors reviewed all related issues and introduced a general IPH model that has been widely applied in previous studies. IPH exists not only in terrestrial networks but also in SatCom, especially for the ISAGNs. In [56], the authors proposed an IPH model for SatCom and

studied the outage probability (OP) and throughput of the system. In [57], the authors explored the ergodic capacity of the ISAGN under the influence of IPH and the NOMA scheme. In [58], the authors explored how IPH impacts LEO SatCom when using the NOMA scheme, with system performance further improved through the deployment of RIS. In [59], the effects of IPH were researched for the ISAGNs with a link selection scheme by using the help of RIS. As is known to the authors, there is a scarcity of studies examining the influence of NOMA and IPH on cognitive ISAGNs, which drives the research in this paper.

C. Contributions

Building on prior discussions, this paper examines the CT of cognitive ISAGNs under NOMA and imperfect conditions, with the system's main contributions outlined as follows

- Firstly, we identified a representative cognitive CT ISAGN, which comprises a satellite, an aerial relay, multiple primary aerial users, two ground destinations, a warden user, and a public user. In particular, the NOMA strategy, the IPH, and CEEs are all investigated for the considered CT system. Based on the authors' knowledge, the considered system can be regarded as the foundational model for the ISAGN with imperfect limitations.
- Secondly, based on the considered system model, the detection error probability (DEP) is obtained using closed-form expressions. Moreover, the OP is also evaluated in closed-form expressions. By analyzing the derived results, we can determine that the IPH and CEEs have significant impacts on CT performance. Especially in scenarios where the system suffers from IPH, a lower bound for the OP emerges at high SNRs, indicating that minimal power is required when IPH is present.
- Thirdly, building on the OP derivations, a closed-form expression for the covert transmission ratio (CTR) is presented for the CT system, enabling the assessment of how critical parameters influence covert performance. Interestingly, we find that the CTR has an upper bound when the CT system is under IPH, which can inform the engineering design of the system. Additionally, an optimization method is implemented in the system to balance power and achieve optimal CT performance.
- Finally, some Monte Carlo (MC) results are carried out to confirm the correctness of the theoretical derivations and verify the effects of imperfect limitations on covert performance. Interestingly, with the system subject to IPH and CEEs, an optimized power allocation strategy is needed to utilize interference for minimizing DEP. Additionally, the OP possesses a lower bound under IPH conditions.

The remainder of this paper is organized as follows. Section II presents the illustrated CT system model under study. Section III discusses the system's covert performance in detail, covering the DEP, the OP, and the CTR, and presents an optimization strategy. Section IV offers representative results to confirm the theoretical findings and explore the effect of critical parameters on CT performance. Finally, Section V summarizes the main conclusion of this research.

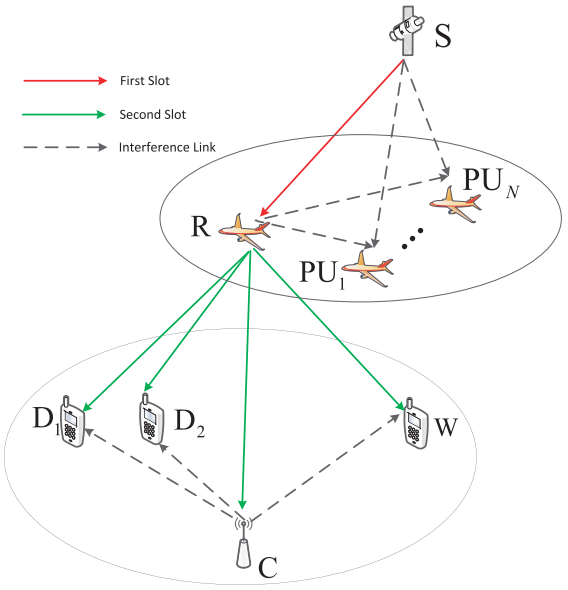

Fig. 1. Description of the system model.

II. System Model

In this paper, a representative covert CISAGN is illustrated, which includes a satellite S, an aerial relay R, two NOMA secondary legitimate users, namely D_1 and D_2, a warden user W, and a public user C. Besides, owing to the cognitive technology, N primary users PU_l, $l \in \{1, \ldots, N\}$. For some practical reasons, there is no direct transmission link between S and D_p, $p \in \{1, 2\}$, which needs the help of R. In addition, C is assumed to work as a full duplex node with two antennas, which means that one antenna receives the signal from R, and the other one is utilized to forward a jamming signal to interfere with the detection probability of D and W. Except for C, each transmission node is provided with a signal antenna. From [35], we know that W can derive the instantaneous CSI of the transmission users. Besides, it is challenging for W to determine where the signal comes from, as W merely derives the distribution of interference.

A. $S \rightarrow R$ Transmission Link

Through the first time slot, the transmitted signal $s(t)$ satisfying $E\left[|s(t)|^2\right] = 1$ from S is forwarded to R. Thus, at R, the obtained signal has the expression as

$$y_R(t) = \sqrt{P_S} h_{SR} \left[s(t) + \delta_S(t)\right] + \eta_R(t), \tag{1}$$

where P_S represents the transmission power of S and h_{SR} denotes the channel coefficient under SR fading. Owing to the NOMA scheme, the signal $s(t)$ can be written as $s(t) = a_1 x_1(t) + a_2 x_2(t)$ with $x_1(t)$ and $x_2(t)$ being the transmitted signal to D_1 and D_2. a_1 and a_2 represent the power allocation (PA) factors satisfying $a_1 > a_2$ in the condition that D_1 is the weaker user. $\delta_S(t)$ denotes the imperfect hardware IPH noise

with the expression as $\delta_S(t) \sim \mathcal{CN}\left(0, k_S^2\right)$, k_S is the IPH level of the transmission node. $\eta_R(t)$ represents the additive white Gaussian noise (AWGN) at R with distribution as $\eta_R(t) \sim \mathcal{CN}\left(0, n_R^2\right)$.

B. $R \rightarrow$ Ground Nodes Link

Through the second time slot, the received signal is forwarded by R to D_p, thus the derived signal from R at D_p has the expression as

$$y_{D_p}(t) = \sqrt{P_R} h_{RD_p} \left[b_1 x_1(t) + b_2 x_2(t) + \delta_R(t)\right] + \sqrt{P_I} h_{CD_p} \left[I(t) + \delta_C(t)\right] + \eta_{D_p}(t), \quad (2)$$

where P_R is the transmission power of R, h_{RD_p} is the channel coefficient between R and D_p which satisfies Rayleigh fading, b_1 and b_2 denote the allocation factors for the second transmission link satisfying $b_1 > b_2$ for the same reason with the first time slot with $b_1^2 + b_2^2 = 1$. $\delta_R(t)$ represents the IPH noise with expression as $\delta_R(t) \sim \mathcal{CN}\left(0, k_R^2 b_1^2 + k_R^2 b_2^2\right)$ with k_R being the IPH level [34]. P_I represents the interference power of I which affects W, h_{CD_p} denotes the channel coefficient between C and D_p, $I(t)$ depicts the interference signal which follows $E\left[|I(t)|^2\right] = 1$, $\delta_C(t)$ represents the IPH noise, with expression as $\delta_C(t) \sim \mathcal{CN}\left(0, k_C^2\right)$ where k_C is the IPH level, $\eta_{D_p}(t)$ depicts the AWGN at D_p which follows $\eta_{D_p}(t) \sim \mathcal{CN}\left(0, n_{D_p}^2\right)$.

After utilizing a similar method, the received signal at C has the expression as

$$y_C(t) = \sqrt{\mathrm{P}_R} h_{RC} \left[b_1 x_1(t) + b_2 x_2(t) + \delta_R(t)\right] + \sqrt{P_{CC}} h_{CC} \left[v_C(t) + \delta_{CC}(t)\right] + \eta_C(t), \quad (3)$$

where h_{RC} represents the channel fading between R and C satisfying Rayleigh model, P_{CC} denotes the interference power due to self-interference in the full-duplex mode. h_{CC} is the channel coefficient for the self-interference undergoing Rayleigh fading. $v_C(t)$ is the self-interference signal satisfying $E\left[|v_C(t)|^2\right] = 1$. $\delta_{CC}(t)$ is the IPH noise, expressed as $\delta_{CC}(t) \sim \mathcal{CN}\left(0, k_{CC}^2\right)$, with k_{CC} being the IPH level [34]. $n_C(t)$ is the AWGN at C which follows $\eta_C(t) \sim \mathcal{CN}\left(0, n_C^2\right)$.

For W, C often sends a noise signal to affect the detection of the covert signal. However, W faces a binary hypothesis testing problem in distinguishing between H_0 and H_1, where H_0 depicts that R does not forward the covert signal, and H_1 denotes that R sends the covert signal. The signal derived at W is expressed as

$$y_W(t) = \begin{cases} \sqrt{P_I} h_{CW} \left[I(t) + \delta_C(t)\right] + \eta_W(t), H_0, \\ \sqrt{P_R} h_{RW} \left[b_1 x_1(t) + b_2 x_2(t) + \delta_R(t)\right] \\ + \sqrt{P_I} h_{CW} \left[I(t) + \delta_C(t)\right] + \eta_W(t), H_1, \end{cases} \quad (4)$$

where h_{CW} denotes the channel coefficient between C and W, $n_W(t)$ is the AWGN at W following $\eta_W(t) \sim \mathcal{CN}\left(0, n_W^2\right)$.

C. Channel Estimation Errors

As discussed in the former section, CEE is one of the non-ideal limitations, thus we have

$$h_B = \widetilde{h}_B + e_{h_B}, B \in \{SR, SP_l, RD, RW\}, \quad (5)$$

where $\widetilde{h}_B$ and h_B denote the estimated and practical channel coefficient respectively. According to [34], $\widetilde{h}_B$ and h_B are considered to have equal ergodicity, e_{h_B} represents the CEE that is orthogonal to $\widetilde{h}_B$ satisfying the expression as

$$e_{h_B} \sim \mathcal{CN}\left(0, \Phi_{e_{h_B}}\right), \quad (6)$$

where

$$\Phi_{e_{h_B}} = \frac{1}{\mathrm{K}_B \overline{\Upsilon}_B + 1}, \quad (7)$$

where K_B represents the length of the estimation symbols and $\overline{\Upsilon_B} = E[\Upsilon_B] = \frac{P_Z E\left[|h_B|^2\right]}{N_\Psi}$, $Z \in \{S, R\}$, $\Psi \in \{R, D, W\}$ denotes the average signal-to-noise (SNR) of the estimation symbols. Besides, $P_Z = (1-\tau) P_{total}$ with $\tau \in \{0, 1\}$ being the scale coefficient. P_{total} depicts the total power with N_Ψ being the AWGN for the transmission nodes.

With the help of [35] and NIH, $\Phi_{e_{h_B}}$ can be written as

$$\Phi_{e_{h_B}} = \frac{\overline{\Upsilon}_{idB} k_Z^2}{\overline{\Upsilon}_{idB}\left(k_Z^2 + \mathrm{K}_B\right) + 1}, \quad (8)$$

where $\overline{\Upsilon}_{idB}$ denotes the SNR of the estimation symbol with ideal hardware and k_Z being the IPH level. $\overline{\Upsilon}_{idB}$ can reflect the precision of the channel estimation derived by the minimum mean square error (MMSE) method.

D. Cognitive Technology

Within the framework of this study, the application of underlay cognitive technology serves as a foundational approach to address. Thus, under the conditions of CEEs and IPH, the interference power at PUs must be maintained below a predetermined threshold P_{total}, the transmitted power at S and R must satisfy the following conditions

$$E\left\{\sum_{l=1}^{N} \sqrt{P_S} \left| \left(\widetilde{h}_{SP_l} + e_{h_{SP_l}}\right) \left[s(t) + \delta_{SP_l}(t)\right] \right|^2 \right\} \leq P_{total}, \quad (9)$$

and

$$E\left\{\sum_{l=1}^{N} \sqrt{P_R} \left| \left(\widetilde{h}_{RP_l} + e_{h_{RP_l}}\right) \left[s(t) + \delta_{RP_l}(t)\right] \right|^2 \right\} \leq P_{total}, \quad (10)$$

where $\delta_{SP_l}(t) \sim \mathcal{CN}\left(0, k_{SP_l}^2\right)$ and $\delta_{RP_l}(t) \sim \mathcal{CN}\left(0, k_{RP_l}^2\right)$ represent the IPH noise at S and R for the cognitive transmission link with k_{SP_l} and k_{RP_l} being the IPH level at PUs. Thus, we have the expression as

$$P_S = \frac{P_{total}}{\sum_{l=1}^{N} \left(\left|\widetilde{h}_{SP_l}\right|^2 + \Phi_{e_{h_{SP_l}}}\right)\left(1 + k_{SP_l}^2\right)}, \quad (11)$$

and

$$P_R = \frac{P_{total}}{\sum_{l=1}^{N} \left(\left|\widetilde{h}_{RP_l}\right|^2 + \Phi_{e_{h_{RP_l}}}\right)\left(1 + k_{RP_l}^2\right)}. \quad (12)$$

E. The Signal-to-Interference Plus Noise and Distortion Error (SINDER) of the Considered System

From (1), after the signal is transmitted to R, the SIC scheme is utilized the meaning that: $x_1(t)$ is first deciphered and then deleted in the received signal. Secondly, $x_2(t)$ will be decoded from the remaining signal. Then, after some mathematical steps, the SINDER of decoding $x_1(t)$ at R has the expression as

$$\gamma_{R,1} = \frac{\lambda_{SR} a_1^2}{\lambda_{SR} AA + \lambda_{SP} BB + CC}, \tag{13}$$

where $\lambda_{SR} = \frac{P_{total}|\widetilde{h}_{SR}|^2}{n_R^2}$, $AA = a_2^2 + a_1^2 k_1^2 + a_2^2 k_2^2$, $\lambda_{SP} = \frac{P_{total}\sum_{l=1}^{N}|\widetilde{h}_{SP_l}|^2}{n_R^2}$, $BB = \left(1+k_{SP_l}^2\right)\left(n_R^2/P_{total}\right)$ and $CC = \frac{P_{total}}{n_R^2}\Phi_{e_{h_{SR}}}\left(a_1^2 + AA\right) + \sum_{l=1}^{N}\Phi_{e_{h_{SP_l}}}\left(1+k_{SP_l}^2\right)$.

Then, by utilizing a similar method, the SINDER for decoding $x_2(t)$ at R has the expression as

$$\gamma_{R,2} = \frac{\lambda_{SR} a_2^2}{\lambda_{SR} AA_1 + \lambda_{SP} BB + CC_1}, \tag{14}$$

where $AA_1 = a_1^2 k_1^2 + a_2^2 k_2^2$ and $CC_1 = \frac{P_{total}}{n_R^2}\Phi_{e_{h_{SR}}}\left(a_2^2 + AA_1\right) + \sum_{l=1}^{N}\Phi_{e_{h_{SP_l}}}\left(1+k_{SP_l}^2\right)$.

It is assumed that the perfect SIC is used at R. To decode the signal $x_1(t)$ for the condition that $\gamma_{R,2}$ could be obtained as $\gamma_{R,1} > \gamma_0$ with γ_0 being the target outage threshold.

With the help of (2) and through the similar steps for deriving (13), the SINDER at D_2 for signal $x_1(t)$ from R is given by

$$\gamma_{D_2,D_1} = \frac{\lambda_{RD_2}}{\lambda_{RD_2}\Theta_1 + \lambda_{RP}\Psi_1 + \lambda_{RP}\lambda_{ID_2}\Phi_1 + \lambda_{ID_2}\mathrm{K}_1 + \mathrm{X}_1}, \tag{15}$$

where $\lambda_{RD_2} = \frac{P_{total}|\widetilde{h}_{RD_2}|^2}{n_{D_2}^2}$, $\lambda_{RP} = \frac{P_{total}\sum_{l=1}^{N}|\widetilde{h}_{RP_l}|^2}{n_{D_2}^2}$, $\lambda_{ID_2} = \frac{P_{total}|\widetilde{h}_{CD_2}|^2}{n_{D_2}^2}$, $\Theta_1 = \frac{b_2^2+k_R^2}{n_{D_2}^2}$, $\Psi_1 = \frac{\left(1+k_{RP_l}^2\right)\left[n_{D_2}^2 + P_I\Phi_{e_{h_{CD_2}}}\left(1+k_C^2\right)\right]}{b_1^2 P_{total}}$, $\Phi_1 = \frac{\left(1+k_C^2\right)\left(1+k_{RP_l}^2\right)n_{D_2}^2}{b_1^2 P_{total}}$, $\mathrm{K}_1 = \frac{\left(1+k_C^2\right)\Phi_{e_{h_{RP_l}}}\left(1+k_{RP_l}^2\right)}{b_1^2}$ and $\mathrm{X}_1 = P_{total}\Phi_{e_{h_{RD_2}}}\left(1+k_R^2\right) + \left[n_{D_2}^2 + P_I\Phi_{e_{h_{CD_2}}}\left(1+k_C^2\right)\right]\Phi_{e_{h_{RP_l}}}\left(1+k_{RP_l}^2\right)$.

By utilizing the similar method of deriving (14), γ_{D_2,D_1} should be satisfied with the condition $\gamma_{D_2,D_1} \geq \gamma_0$, D_2 can distinguish whether the signal comes from its own antenna and delete its own signal, thus the SINDER at D_2 for $x_2(t)$ from R can be written as

$$\gamma_{D_2,D_2} = \frac{\lambda_{RD_2}}{\lambda_{RD_2}\Theta_2 + \lambda_{RP}\Psi_2 + \lambda_{RP}\lambda_{ID_2}\Phi_2 + \lambda_{ID_2}\mathrm{K}_2 + \mathrm{X}_1}, \tag{16}$$

where $\Theta_2 = \frac{k_R^2}{n_{D_2}^2}$, $\Psi_2 = \frac{\left(1+k_{RP_l}^2\right)\left[n_{D_2}^2 + P_I\Phi_{e_{h_{CD_2}}}\left(1+k_C^2\right)\right]}{b_2^2 P_{total}}$, $\Phi_2 = \frac{\left(1+k_C^2\right)\left(1+k_{RP_l}^2\right)n_{D_2}^2}{b_2^2 P_{total}}$ and $\mathrm{K}_2 = \frac{\left(1+k_C^2\right)\Phi_{e_{h_{RP_l}}}\left(1+k_{RP_l}^2\right)}{b_2^2}$.

Then, at D_1, the transmitted signal $x_1(t)$ can be detected while regarding the $x_2(t)$ as a noise, thus the SINDER at D_1 from R has the expression as

$$\gamma_{D_1,D_1} = \frac{\lambda_{RD_1}}{\lambda_{RD_1}\Theta_3 + \lambda_{RP}\Psi_3 + \lambda_{RP}\lambda_{ID_1}\Phi_3 + \lambda_{ID_1}\mathrm{K}_3 + \mathrm{X}_3}, \tag{17}$$

where $\lambda_{RD_1} = \frac{P_{total}|\widetilde{h}_{RD_1}|^2}{n_{D_1}^2}$, $\lambda_{ID_1} = \frac{P_{total}|\widetilde{h}_{CD_1}|^2}{n_{D_1}^2}$, $\Theta_3 = \frac{b_2^2+k_R^2}{n_{D_1}^2}$, $\Psi_3 = \frac{\left(1+k_{RP_l}^2\right)\left[n_{D_1}^2 + P_I\Phi_{e_{h_{CD_1}}}\left(1+k_C^2\right)\right]}{b_1^2 P_{total}}$, $\Phi_3 = \frac{\left(1+k_C^2\right)\left(1+k_{RP_l}^2\right)n_{D_1}^2}{b_1^2 P_{total}}$, $\mathrm{K}_3 = \frac{\left(1+k_C^2\right)\Phi_{e_{h_{RP_l}}}\left(1+k_{RP_l}^2\right)}{b_1^2}$ and $\mathrm{X}_3 = P_{total}\Phi_{e_{h_{RD_1}}}\left(1+k_R^2\right) + \left[n_{D_1}^2 + P_I\Phi_{e_{h_{CD_1}}}\left(1+k_C^2\right)\right]\Phi_{e_{h_{RP_l}}}\left(1+k_{RP_l}^2\right)$.

Thus, with the DF protocol, the final SINDER for decoding $x_1(t)$ of the system has the expression as

$$\gamma_{D_1} = \min\left[\gamma_{R,1}, \min\left(\gamma_{D_2,D_1}, \gamma_{D_1,D_1}\right)\right]. \tag{18}$$

By using the similar method, the final SINDER for decoding $x_2(t)$ of the system can be written as

$$\gamma_{D_2} = \min\left(\gamma_{R,2}, \gamma_{D_2,D_2}\right). \tag{19}$$

Finally, the final SINDER of the system is shown as

$$\gamma_e = \min\left(\gamma_{D_1}, \gamma_{D_2}\right). \tag{20}$$

From (3) and without considering the CEE, the SINDER for C can be derived as

$$\gamma_C = \frac{\lambda_{RC}}{\lambda_{RC} k_R^2 + \lambda_{CC}\left(1+k_{CC}^2\right) + 1}, \tag{21}$$

where $\lambda_{RC} = \frac{P_R|h_{RC}|^2}{n_C^2}$ and $\lambda_{CC} = \frac{P_{CC}|h_{CC}|^2}{n_C^2}$.

By the same way, the SINDER for (4) can be obtained as

$$\gamma_W = \begin{cases} \lambda_{CW}\left(1+k_C^2\right) + 1, \\ \dfrac{\lambda_{RW}\left(1+k_R^2\right)P_{total}/n_W^2}{\lambda_{RP}\left(1+k_{RP_l}^2\right) + T} + \dfrac{T_1\left(1+k_R^2\right)P_{total}/n_W^2}{\lambda_{RP}\left(1+k_{RP_l}^2\right) + T} \\ +\lambda_{CW}\left(1+k_C^2\right) + 1, \end{cases} \tag{22}$$

where $\lambda_{CW} = \frac{P_I|h_{CW}|^2}{n_w^2}$, $\lambda_{RW} = \frac{P_{total}|\widetilde{h}_{RW}|^2}{n_W^2}$, $T = \frac{P_{total}\Phi_{e_{h_{RP_l}}}\left(1+k_{RP_l}^2\right)}{n_W^2}$ and $T_1 = \frac{P_{total}\Phi_{e_{h_{RW}}}\left(1+k_R^2\right)}{n_W^2}$.

III. Covert Performance of Considered System

In this part, a thorough analysis is conducted on the covert performance characteristics of the considered system. In the very beginning, the channel descriptions for the terrestrial transmission links and satellite transmission links are provided.

A. The Terrestrial Transmission Links

By utilizing the method of [35], the PDF and CDF for λ_Q, $Q \in \{RD_p, RC, RW, CW\}$ are, respectively, given by

$$f_{\lambda_Q}(x) = \frac{1}{\overline{\lambda}_Q} e^{-\frac{x}{\overline{\lambda}_Q}}, \tag{23}$$

and

$$F_{\lambda_Q}(x) = 1 - e^{-\frac{x}{\overline{\lambda}_Q}}, \tag{24}$$

where $\overline{\lambda}_Q$ denotes the average SNR for the channel fading.

With the help of [35], the PDF for λ_{RP} can be written as

$$f_{\lambda_{RP}}(x) = \sum_{\tau=1}^{\rho(A_{RP})} \sum_{\omega=1}^{\xi_\tau(A_{RP})} \frac{\Omega_{\tau,\omega}(A_{RP})}{(\omega-1)!\overline{\lambda}_{\langle\tau\rangle}^{\omega}} x^{\omega-1} e^{-x/\overline{\lambda}_{\langle\tau\rangle}}, \tag{25}$$

where $A_{RP} = \text{diag}\left(\overline{\lambda}_{\langle 1\rangle}, \ldots, \overline{\lambda}_{\langle\tau\rangle}, \ldots \overline{\lambda}_{\langle N\rangle}\right)$, $\rho(A_{RP})$ is the number of the distinct diagonal elements of A_{RP}, $\overline{\lambda}_{\langle 1\rangle} < \overline{\lambda}_{\langle\tau\rangle}, \ldots < \overline{\lambda}_{\langle N\rangle}$ represents the ascending order of $\overline{\lambda}_{\langle\tau\rangle}$, $\xi_\tau(A_{RP})$ depicts the variety of $\overline{\lambda}_{\langle\tau\rangle}$, $\Omega_{\tau,\omega}(A_{RP})$ is the τ,ω-th element of A_{RP}.

Then, with the help of (25) and [63], the CDF for λ_{RP} can be written as

$$F_{\lambda_{RP}}(x) = 1 - \sum_{\tau=1}^{\rho(A_{RP})} \sum_{\omega=1}^{\xi_\tau(A_{RP})} \sum_{\varepsilon=1}^{\omega-1} \frac{\Omega_{\tau,\omega}(A_{RP})}{(\omega-1)!} \left(\frac{x}{\overline{\lambda}_{\langle\tau\rangle}}\right)^{\varepsilon} e^{-x/\overline{\lambda}_{\langle\tau\rangle}}. \tag{26}$$

B. The Satellite Transmission Links

In this study, the geosynchronous Earth orbit (GEO) serves as a case example. Besides, time division multiple access (TDMA) is utilized in this paper, which means that only one antenna is used at a time slot. The channel coefficients $h_U, U \in \{SR, SP_l\}$ between the satellite beam and the UAVs can be written as

$$\widetilde{h}_U = \varpi_U f_U, \tag{27}$$

where f_U denotes the random SR factor of the satellite transmission link, ϖ_U is affected by free space loss (FSL) and antenna pattern, which has the expression as

$$\varpi_U = \frac{c}{8\pi^2 f}\sqrt{\frac{R_U R_D}{d_0^2 + d^2}}, \tag{28}$$

where c denotes the transmission speed of the light, f represents the utilized frequency of the system, d is the distance between the satellite beam and the UAV, $d_0 = 3.6 \times 10^4$Km. R_U depicts the satellite beam gain and R_D represents the receive antenna gain.

With the help of [60], the receive antenna gain R_D can be nearly shown as

$$R_D(dB) \simeq \begin{cases} \overline{G}_{\max}, & for\ 0 < \vartheta < \pi/180 \\ 32 - 25\log\dfrac{180\vartheta}{\pi}, & for\ \pi/180 < \vartheta < 4\pi/15 \\ -10, & for\ 4\pi/15 < \vartheta \le \pi, \end{cases} \tag{29}$$

where $\overline{G}_{\max}$ shows the largest beam gain with ϑ as the angle.

R_U depicts the satellite beam gain, thus, R_U has the following expression as

$$R_U \simeq R_U^{\max}\left[36\frac{J_3(\chi)}{\chi^3} + \frac{J_1(\chi)}{2\chi}\right]^2, \tag{30}$$

where $R_U^{\max}$ depicts the maximal value for the beam gain with $\chi = 2.07123\sin\beta/\sin\beta_{3\text{dB}}$ and β being the angle. $\beta_{3\text{dB}}$ represents the 3dB angle. $J_3(\cdot)$ and $J_1(\cdot)$ depict the Bessel function for first kind. Furthermore, $\beta \to 0$ is considered. On this foundation, $R_U \approx R_U^{max}$ can be derived. Above all, we assume $\widetilde{h}_U = \varpi_U^{\max} f_U$ with $\varpi_U^{\max} = \frac{c}{8\pi^2 f}\sqrt{\frac{R_U^{\max} R_D}{d_0^2 + d^2}}$.

Then, by utilizing (30) and (27), the PDF for $\lambda_U = \overline{\lambda}_U\left|\varpi_U^{\max} f_U\right|^2$ can be shown as

$$f_{\lambda_U}(x) = \alpha_U \sum_{k_U=0}^{\varsigma_U-1} \frac{(-\phi_U)^{k_U}(1-\varsigma_U)_{k_U}}{(k_U!)^2\left(\bar{\lambda}_U\right)^{k_U+1}} x^{k_U} e^{-\Delta_U x}, \tag{31}$$

where $\bar{\lambda}_U$ represents the average SNR from the satellite source, $\Delta_U = \frac{\varphi_U - \phi_U}{\bar{\lambda}_U}$, $\alpha_U = \frac{2\omega_U^{\varsigma_U}\xi_U^{\varsigma_U}}{(2\omega_U\varsigma_U+\psi_U)^{\varsigma_U}2\omega_U}$, $\varphi_U = \frac{1}{2\omega_U}$, $\phi_U = \frac{\psi_U}{2\omega_U(2\omega_U\varsigma_U+\psi_U)}$ with $\varsigma_U > 0$ denoting the fading severity parameter, ω_U depicts the mean power of the multiple factors, ψ_U represents the mean power of the line of sight (LOS) element. Throughout the whole paper, we take ς_U being an integer, for example. $(\cdot)_x$ depicts the Pochhammer symbol [63].

With the assistance of [23] and through several mathematical steps, the CDF for λ_U can be written as

$$F_{\lambda_U}(x) = 1 - \alpha_U \sum_{k_U=0}^{\varsigma_U-1}\sum_{q=0}^{k_U} \frac{(-\phi_U x)^{k_U}(1-\varsigma_U)_{k_U} x^q \exp(-\Delta_U x)}{(k_U!)\left(\bar{\lambda}_U\right)^{k_U+1} q!\Delta_U^{k_U-q+1}}. \tag{32}$$

Then, by utilizing the help of [35], the PDF for λ_{SP} has the expression as

$$f_{\lambda_{SP}}(x) = \sum_{k_1=0}^{\varsigma_{SP}-1} \cdots \sum_{k_N=0}^{\varsigma_{SP}-1} \Xi(N)\, x^{\Lambda_{SP}-1} e^{-\Delta_{SP}x}, \tag{33}$$

where $\Xi(N) \triangleq \prod_{\sigma=1}^{N} \partial(\varsigma_\sigma)\alpha_{SP}^N \prod_{\wp=1}^{N-1} B\left(\sum_{\ell=1}^{\wp}\varsigma_\ell + \wp, \varsigma_{\wp+1}+1\right)$, $\Lambda_{SP} \triangleq \sum_{\hbar=1}^{N}\varsigma_\hbar + N$, $\partial(\varsigma_\sigma) = \frac{(1-\varsigma_{SP})_{\varsigma_\sigma}(-\phi_{SP})^{\varsigma_\sigma}}{(\varsigma_\sigma!)^2\bar{\lambda}_{SP}^{\varsigma_\sigma+1}}$, $\Delta_{SP} = \frac{\varphi_{SP}-\phi_{SP}}{\bar{\lambda}_{SP}}$, $\alpha_{SP} = \frac{2\omega_{SP}^{\varsigma_{SP}}\xi_{SP}^{\varsigma_{SP}}}{(2\omega_{SP}\varsigma_{SP}+\psi_{SP})^{\varsigma_{SP}}2\omega_{SP}}$, $\varphi_{SP} = \frac{1}{2\omega_{SP}}$, $\phi_{SP} = \frac{\psi_{SP}}{2\omega_{SP}(2\omega_{SP}\varsigma_{SP}+\psi_{SP})}$ and $B(,.,)$ depicts the Beta function [63].

C. Detection Evaluation at W

During this subsection, W judges whether there is a covert communication between R and D in detail. The performance metric for the CT is DEP, which results from the binary hypothesis testing problem faced by W. In particular, W needs to value whether the CT occurs or not in cases H_0, H_1, and

derive the binary detection results D_0 and D_1. It is assumed that the prior probabilities of H_0 and H_1 are equal, then the DEP can be written as

$$P_{DEP}(\gamma_0) = P_{FA}(\gamma_0) + P_{MD}(\gamma_0), \tag{34}$$

where $P_{FA}(\gamma_0)$ depicts the false alarm probability (FAP) and $P_{MD}(\gamma_0)$ represents the missed detection probability (MDP) with γ_0 being the threshold, which can be shown as

$$P_{FA}(\gamma_0) = \Pr(D_1 | H_0), \tag{35a}$$

and

$$P_{MD}(\gamma_0) = \Pr(D_0 | H_1), \tag{35b}$$

where $P_{FA}(\gamma_0)$ represents that R does not really transmit the signal but W incorrectly judges that the signal is sent, however, $P_{MD}(\gamma_0)$ means that R sends the signal but W does not find it. It can be easily seen that, $0 \le P_{DEP}(\gamma_0) \le 1$ with $P_{DEP}(\gamma_0) = 0$ being that W correctly detects the CT between R and D all the time, while $P_{DEP}(\gamma_0) = 1$ denotes that W can not correctly detect the CT of the system. In the following **Theorem 1**, the expressions for FAP and MDP will be provided.

Theorem 1: The DEP of the considered CT systems can be divided into two parts, namely, $P_{FA}(\gamma_0)$ and $P_{MD}(\gamma_0)$, which are, respectively, shown as

$$P_{FA}(\gamma_0) = \begin{cases} 1, & \gamma_0 < 1 \\ 1 - e^{-\frac{\gamma_0 - 1}{1 + k_C^2}}, & \gamma_0 \ge 1, \end{cases} \tag{37}$$

and

$$P_{MD}(\gamma_0) = \begin{cases} 0, & \gamma_0 < 1 \\ \mathcal{Q}_1(\gamma_0) - \mathcal{Q}_2(\gamma_0) + \mathcal{Q}_3(\gamma_0), & 1 \le \gamma_0 \le \gamma_1 \\ \mathcal{P}_1(\gamma_0) - \mathcal{P}_2(\gamma_0) + \mathcal{P}_3(\gamma_0), & \gamma_0 > \gamma_1. \end{cases} \tag{38}$$

where $\gamma_1 = 1 + \frac{T_1 P_{total}(1 + k_R^2)}{T n_W^2}$,

$$\mathcal{Q}_1(\gamma_0) = \frac{\Gamma(N, GZ)}{(N-1)!} - \frac{\exp\left(-\frac{T_6}{\bar{\lambda}_{RW} T_3}\right) Z^N}{(N-1)!} \Gamma(N, G), \tag{39}$$

where $Z = \frac{\bar{\lambda}_{RW} T_3}{\bar{\lambda}_{RW} T_3 + \bar{\lambda}_{RP} T_5}$, $G = -\frac{T_6}{Z T_5 \bar{\lambda}_{RP}}$.

$$\mathcal{P}_1(\gamma_0) = 1 - \exp\left(-\frac{T_6}{T_3 \bar{\lambda}_{RW}}\right)\left(\frac{T_3 \bar{\lambda}_{RW}}{T_3 \bar{\lambda}_{RW} + T_5 \bar{\lambda}_{RP}}\right)^N, \tag{40}$$

$$\mathcal{P}_3(\gamma_0) = \exp\left(-\frac{T_6}{\bar{\lambda}_{RW} T_3}\right)\left[\left(\frac{\bar{\lambda}_{RW} T_3}{\bar{\lambda}_{RW} T_3 + \bar{\lambda}_{RP} T_5}\right)^N + \frac{\bar{\lambda}_{RW} T_3}{\bar{\lambda}_{RP}^N \bar{\lambda}_{CW} T_2 (N-1)!} H(N-1, X, Y)\right], \tag{41}$$

where $X = \frac{\bar{\lambda}_{RW} T_3 + \bar{\lambda}_{RP} T_5}{\bar{\lambda}_{RW} T_3 \bar{\lambda}_{RP}}$, $Y = \frac{T_4 \bar{\lambda}_{CW} - \bar{\lambda}_{RW} T_3}{\bar{\lambda}_{CW} T_2}$,

$$H(n, \mu, \beta) = (-1)^{n-1} \beta^n e^{\beta\mu} \mathrm{Ei}(-\beta\mu) + \sum_{-\lambda=1}^{n} (-\lambda - 1)! (-\beta)^{n - -\lambda} \mu^{--\lambda}, \tag{42}$$

and

$$L(a, b, c, d, e, f, g, h, i) = \int_a^\infty x^b \exp\left(-cx - \frac{d}{ex + f}\right) \frac{gx + h}{gx + h - i} dx. \tag{43}$$

and $T_2 = \left(1 + k_{RP_l}^2\right)\left(1 + k_C^2\right)$, $T_3 = \left(1 + k_R^2\right) P_{total} / n_W^2$, $T_4 = \left(1 + k_C^2\right) T$, $T_5 = \left(1 + k_{RP_l}^2\right)(\gamma_0 - 1)$, $T_6 = T(\gamma_0 - 1) - T_1\left(1 + k_R^2\right) P_{total} / n_W^2$ with $\mathrm{Ei}(x)$ being the Exponential integral function defined in [63].

Proof: The detailed proof can be seen in Appendix A. □

D. Outage Performance of The System

It is noteworthy that OP is a crucial metric for evaluating system performance and serves as the basis for the covert transmission rate. The OP is defined as the probability that the SINDER of the system drops below a specified threshold γ_0. With the help of (20), the OP has the expression as

$$\begin{aligned} P_{out}(\gamma_0) &= \Pr(\gamma_e \le \gamma_0) = \Pr\left[\min\left(\gamma_{D_1}, \gamma_{D_2}\right) \le \gamma_0\right] \\ &= \Pr\left(\gamma_{D_1} \le \gamma_0\right) + \Pr\left(\gamma_{D_2} \le \gamma_0\right) \\ &\quad - \Pr\left(\gamma_{D_1} \le \gamma_0\right) \Pr\left(\gamma_{D_2} \le \gamma_0\right), \end{aligned} \tag{44}$$

Theorem 2: The OP of the considered system is shown as

$$\begin{aligned} \Pr\left(\gamma_{D_1} \le \gamma_0\right) &= \Pr\left(\gamma_{R,1} \le \gamma_0\right) + P_2(\gamma_0) \\ &\quad - \Pr\left(\gamma_{R,1} \le \gamma_0\right) P_2(\gamma_0), \end{aligned} \tag{45}$$

and

$$\begin{aligned} \Pr\left(\gamma_{D_2} \le \gamma_0\right) &= \Pr\left(\gamma_{R,2} \le \gamma_0\right) + \Pr\left(\gamma_{D_2, D_2} \le \gamma_0\right) \\ &\quad - \Pr\left(\gamma_{R,2} \le \gamma_0\right) \Pr\left(\gamma_{D_2, D_2} \le \gamma_0\right), \end{aligned} \tag{46}$$

where

$$\begin{aligned} &\Pr\left(\gamma_{D_2, D_2} \le \gamma_0\right) \\ &= 1 - \frac{\bar{\lambda}_{RD_2}(1 - \Theta_2 \gamma_0)}{(N-1)!\left(\bar{\lambda}_{RP}\right)^N} \\ &\quad \times \frac{\exp\left[-\frac{\gamma_0 \mathrm{X}_1}{\bar{\lambda}_{RD_2}(1 - \Theta_2 \gamma_0)}\right]}{\bar{\lambda}_{ID_2} \gamma_0 \Phi_2} \times H(N-1, \mu_2, \beta_2), \end{aligned} \tag{47}$$

where $\mu_2 = \frac{\bar{\lambda}_{RD_2}(1 - \Theta_2 \gamma_0) + \bar{\lambda}_{RP} \gamma_0 \Psi_2}{\bar{\lambda}_{RP} \bar{\lambda}_{RD_2}(1 - \Theta_2 \gamma_0)}$, $\beta_2 = \frac{\bar{\lambda}_{ID_2} \gamma_0 \mathrm{K}_2 + \bar{\lambda}_{\mathrm{RD}_2}(1 - \Theta_2 \gamma_0)}{\bar{\lambda}_{ID_2} \gamma_0 \Phi_2}$.

The expressions of $P_2(\gamma_0)$, $\Pr(\gamma_{R,1} \le \gamma_0)$ and $\Pr(\gamma_{R,2} \le \gamma_0)$ are shown in (36), at the bottom of the page, (56) and (57), shown at the bottom of the next page, where

$$\nu(k_1) = \frac{\alpha_{SP}(1-\varsigma_{SP})_{k_1}(-\phi_{SP})^{k_1}}{(k_1!)^2\left(\overline{\lambda}_{SP}\right)^{k_1+1}}, \tag{48}$$

$$\nu(k_2) = \frac{\alpha_{SP}(1-\varsigma_{SP})_{k_2}(-\phi_{SP})^{k_2}}{(k_2!)^2\left(\overline{\lambda}_{SP}\right)^{k_2+1}} B(k_1+1, k_2+1), \tag{49}$$

$$\nu(k_3) = \frac{\alpha_{SP}(1-\varsigma_{SP})_{k_3}(-\phi_{SP})^{k_3}}{(k_3!)^2\left(\overline{\lambda}_{SP}\right)^{k_3+1}} B(k_1+k_2+2, k_3+1), \tag{50}$$

Proof: The detailed proof can be seen in Appendix B. □

E. Covert Transmission Rate of The System

Covert transmission rate is also a crucial factor in assessing the reliability of the system. According to [61], CTR represents the optimal transmission rate between the satellite and the legitimate NOMA users, ensuring the warden's detection is avoided.

Theorem 3: The CTR of the considered system is shown as (51) and (52), where x_i represents the i-th zero of Legendre Polynomials, and ω_i depicts the weight factors from Table (25.4) in [62].

$$R_{D_1} = \log_2\left(1+\gamma_D^{\max}\right) P_2\left(\gamma_D^{\max}\right) - \frac{\gamma_D^{\max}}{2\ln 2}\sum_{i=1}^{n}\omega_i \frac{P_2(x_i)}{1+x_i}, \tag{51}$$

$$R_{D_2} = \log_2\left(1+\gamma_D^{\max}\right)\Pr\left(\gamma_{D_2D_2} \le \gamma_D^{\max}\right) - \frac{\gamma_D^{\max}}{2\ln 2}\sum_{i=1}^{n}\omega_i \frac{\Pr\left(\gamma_{D_2D_2} \le x_i\right)}{1+x_i}, \tag{52}$$

where $\gamma_D^{\max} = \min\left[\min\left(\frac{1}{\Theta_1}, \frac{1}{\Theta_3}\right), \frac{1}{\Theta_2}\right]$.

Proof: The detailed proof can be seen in Appendix C. □

F. Optimazition for DEP

To optimize the system's power balance and achieve the best CT performance, we formulated an optimization problem aimed at minimizing the DEP, while using the convex optimization method with the optimization steps as

$$\min_{a_1,b_1,\tau} \; P_{DEP}(\gamma_0) = P_{FA}(\gamma_0) + P_{MD}(\gamma_0) \tag{58a}$$

$$\text{s.t. } P_S \le P_S^{\max}, \tag{58b}$$

$$P_R \le P_R^{\max}, \tag{58c}$$

$$a_1 \in (0.5, 1), \tag{58d}$$

$$b_1 \in (0.5, 1), \tag{58e}$$

$$\tau \in (0, 1). \tag{58f}$$

where (58a) is DEP as the objective function, (58b) and (58c) limit the transmission power of the satellite and UAV, respectively. Besides, (58d) and (58e) impose restrictions on the range of values for the NOMA power allocation factors. Furthermore, (58f) represents the scale coefficient of the total system power. These constraints are introduced to ensure that the optimization process remains practical and feasible within the physical limitations of the system. The transmission power limits for the satellite and UAV prevent a waste of energy, ensuring that the hardware operates within its energy budget while maintaining reliable communication links. Specifically, the satellite's power constraint ensures that the transmission power does not surpass its power generation and radiation limits, while the UAV's power constraint ensures that it does not exceed the available battery capacity, which could lead to premature failure or inefficient operations. Moreover, the constraints on the NOMA power allocation factors a_1 and b_1 ensure that power is distributed optimally between users. Finally, the scale coefficient τ serves to manage the total system power, ensuring that it remains within a reasonable operating range to avoid excessive energy consumption while maintaining the desired communication performance.

To tackle this optimization challenge, convex optimization techniques are used due to the convexity of both the objective function and the constraint conditions. The transmission power functions, as well as the NOMA allocation factors and the scale coefficient, exhibit convex properties, which allow us to apply efficient convex optimization solvers. By using methods such as interior-point algorithms or gradient-based

$$P_2(\gamma_0) = 2 - \frac{\overline{\lambda}_{RD_2}(1-\Theta_1\gamma_0)}{(N-1)!\left(\overline{\lambda}_{RP}\right)^N}\frac{\exp\left[-\frac{\gamma_0 X_1}{\overline{\gamma}_{RD_2}(1-\Theta_1\gamma_0)}\right]}{\overline{\lambda}_{ID_2}\gamma_0\Phi_1} H(N-1, \mu_1, \beta_1) - \frac{\overline{\lambda}_{RD_1}(1-\Theta_3\gamma_0)}{(N-1)!\left(\overline{\lambda}_{RP}\right)^N}\frac{\exp\left[-\frac{\gamma_0 X_3}{\overline{\lambda}_{RD_1}(1-\Theta_3\gamma_0)}\right]}{\overline{\lambda}_{ID_1}\gamma_0\Phi_3}$$
$$\times H(N-1, \mu_3, \beta_3) - \left[1 - \frac{\overline{\lambda}_{RD_2}(1-\Theta_1\gamma_0)}{(N-1)!\left(\overline{\lambda}_{RP}\right)^N}\frac{\exp\left[-\frac{\gamma_0 X_1}{\overline{\gamma}_{RD_2}(1-\Theta_1\gamma_0)}\right]}{\overline{\lambda}_{ID_2}\gamma_0\Phi_1} H(N-1, \mu_1, \beta_1)\right]$$
$$\times \left[1 - \frac{\overline{\lambda}_{RD_1}(1-\Theta_3\gamma_0)}{(N-1)!\left(\overline{\lambda}_{RP}\right)^N}\frac{\exp\left[-\frac{\gamma_0 X_3}{\overline{\lambda}_{RD_1}(1-\Theta_3\gamma_0)}\right]}{\overline{\lambda}_{ID_1}\gamma_0\Phi_3} H(N-1, \mu_3, \beta_3)\right]. \tag{36}$$

optimization, we can effectively determine the optimal values for the decision variables a_1, b_1, and τ that minimize the DEP while respecting all system constraints.

IV. Numerical Results

In this section, Monte Carlo numerical results are presented, further validating the correctness of our conclusions. For the sake of simplicity in calculations, the system parameters are set as $\overline{\lambda}_{RP} = \overline{\lambda}_{RW} = \overline{\lambda}_{SR} = \overline{\lambda}_{RD_p} = \overline{\gamma}$, $\overline{\lambda}_{CW} = \overline{\lambda}_{ID_p} = \overline{\gamma}_I$, $n_W^2 = n_{D_p}^2 = n_C^2 = n_R^2 = 1$, $k_R = k_C = k_{CC} = k_{SP_l} = k_{RP_l} = k$. Besides, Table I shows the channel parameters for the considered system.

TABLE I
Channel and System Parameters

Shadowing Type	ς_U	ω_U	ψ_U
Frequent heavy shadowing (FHS)	1	0.063	0.0007
Average shadowing (AS)	5	0.251	0.279
Infrequent light shadowing (ILS)	10	0.158	1.29
Channel Parameters			
Frequency band	$f = 2$ GHz		
Maximal beam gain	$R_U^{\max} = 48$ dB		
3dB angle	$\beta_{3\text{dB}} = 0.8^\circ$		

Fig. 2 depicts the DEP via different γ_0 and different k with $N = 3$, $\bar{\gamma}_I = 0$dB, $P_{total} = 25$dB. The theoretical analysis is validated by the MC simulation results, demonstrating the correctness of our theoretical derivation. As shown in the figure, DEP first decreases and then increases with respect to γ_0, resulting in a minimum value. Additionally, there exists an optimal threshold, corresponding to the γ_0 at this minimum, such that if the warden adjusts his detection threshold to this value, the DEP will significantly decrease. Furthermore, the HIs level has little effect on the DEP in the regions on both sides, but has a considerable impact on the warden's minimum DEP and optimal detection threshold.

Fig. 3 illustrates the DEP via different τ, different γ_0, and different $\overline{\gamma}$ with $N = 3$, $\bar{\gamma}_I = 0$dB, $P_{total} = 25$dB. As observed, the trend of DEP with respect to the warden's detection threshold in this figure is consistent with that in the previous one. Furthermore, the power allocation factor τ

$$\mathcal{Q}_2(\gamma_0) = \frac{\exp\left(-\frac{T_6}{T_3\overline{\lambda}_{RW}}\right)}{\overline{\lambda}_{RP}^N (N-1)!}\left[\overline{\lambda}_{RW}^{N-1} Z^N \Gamma(N, G) + L\left(-\frac{T_6}{T_5}, N-1, \frac{1}{Z\overline{\lambda}_{RP}}, 0, 0, 0, \overline{\lambda}_{CW}T_2, \overline{\lambda}_{CW}T_4, \overline{\lambda}_{RW}T_3\right)\right]. \tag{53}$$

$$\mathcal{Q}_3(\gamma_0) = \frac{\exp\left(-\frac{T_6}{\overline{\lambda}_{RW}T_3}\right)}{\overline{\lambda}_{RP}^N (N-1)!} L\left(-\frac{T_6}{T_5}, N-1, X, 0, 0, 0, \overline{\lambda}_{CW}T_2, \overline{\lambda}_{CW}T_4, \overline{\lambda}_{RW}T_3\right). \tag{54}$$

$$\mathcal{P}_2(\gamma_0) = \frac{\exp\left(-\frac{T_5}{T_2\overline{\lambda}_{CW}}\right)}{\overline{\lambda}_{RP}^N (N-1)!} L\left(0, N-1, \bar{\lambda}_{RP}, T_6 - \frac{T_4T_5}{T_2}, \bar{\lambda}_{CW}T_2, \bar{\lambda}_{CW}T_4, \bar{\lambda}_{CW}T_2, \bar{\lambda}_{CW}T_4, \bar{\lambda}_{RW}T_3\right). \tag{55}$$

$$\begin{aligned}\Pr\left(\gamma_{R,1} \le \gamma_0\right) = &\sum_{k_{SR}=0}^{\varsigma_{SR}-1} \frac{\alpha_{SR}(-\phi_{SR})^{k_{SR}}(1-\varsigma_{SR})_{k_{SR}}}{(k_{SR}!)^2\left(\bar{\lambda}_{SR}\right)^{k_{SR}+1}} \sum_{k_1=0}^{\varsigma_{SP}-1}\sum_{k_2=0}^{\varsigma_{SP}-1}\sum_{k_3=0}^{\varsigma_{SP}-1} \nu(k_1)\nu(k_2)\nu(k_3) \sum_{q=0}^{k_{SR}}\sum_{v=0}^{q}\binom{q}{v}\left(\frac{CC\gamma_0}{a_1^2 - AA\gamma_0}\right)^{q-v} \\ &\times\left(\frac{BB\gamma_0}{a_1^2 - AA\gamma_0}\right)^{v} \exp\left(-\frac{\Delta_{SR}\gamma_0 CC}{a_1^2 - AA\gamma_0}\right)\Gamma(v+k_1+k_2+k_3+3)\left(\Delta_{SP} + \frac{\Delta_{SR}\gamma_0 BB}{a_1^2 - AA\gamma_0}\right)^{-v-k_1-k_2-k_3-3}.\end{aligned} \tag{56}$$

$$\begin{aligned}\Pr\left(\gamma_{R,2} \le \gamma_0\right) = &\sum_{k_{SR}=0}^{\varsigma_{SR}-1} \frac{\alpha_{SR}(-\phi_{SR})^{k_{SR}}(1-\varsigma_{SR})_{k_{SR}}}{(k_{SR}!)^2\left(\bar{\lambda}_{SR}\right)^{k_{SR}+1}} \sum_{k_1=0}^{\varsigma_{SP}-1}\sum_{k_2=0}^{\varsigma_{SP}-1}\sum_{k_3=0}^{\varsigma_{SP}-1} \nu(k_1)\nu(k_2)\nu(k_3) \sum_{q=0}^{k_{SR}}\sum_{v=0}^{q}\binom{q}{v}\left(\frac{BB\gamma_0}{a_2^2 - AA_1\gamma_0}\right)^{q} \\ &\times\left(\frac{CC_1}{BB}\right)^{v} \exp\left(-\frac{\Delta_{SR}\gamma_0 CC_1}{a_2^2 - AA_1\gamma_0}\right)\Gamma(k_1+k_2+k_3+3+q-v)\left(\Delta_{SP} + \frac{\Delta_{SR}\gamma_0 BB}{a_2^2 - AA_1\gamma_0}\right)^{-k_1-k_2-k_3-3+v-q}.\end{aligned} \tag{57}$$

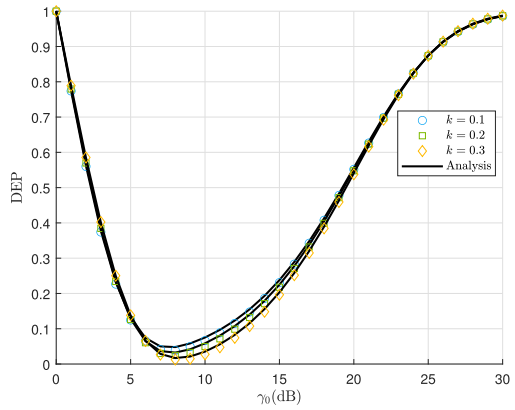

Fig. 2. DEP versus γ_0 under different k with $N = 3$, $\bar{\gamma}_I = 0$dB, $P_{total} = 25$dB.

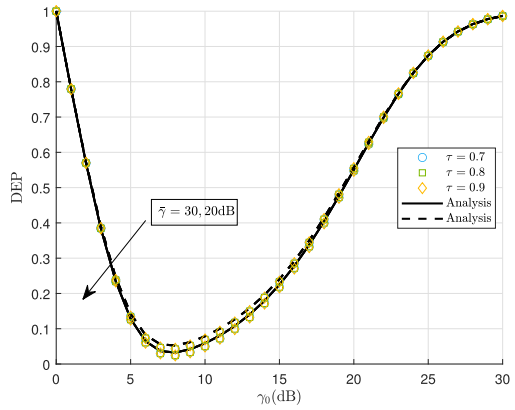

Fig. 3. DEP versus γ_0 under different τ with $N = 3$, $\bar{\gamma}_I = 0$dB, $P_{total} = 25$dB.

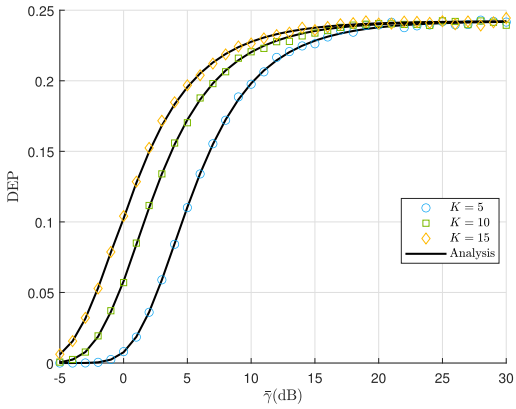

Fig. 4. DEP versus $\overline{\gamma}$ under different K with $N = 3$, $\tau = 0.7$, $k = 0.1$, $P_{total} = 25$dB, $\bar{\gamma}_I = -25$dB.

has little effect on the DEP across various threshold values. In addition, a larger $\overline{\gamma}$ leads to a reduction in DEP.

Fig. 4 shows the DEP via different $\overline{\gamma}$ and different K with $N = 3$, $\tau = 0.7$, $k = 0.1$, $P_{total} = 25$dB, $\bar{\gamma}_I = -25$dB. As $\overline{\gamma}$ increases, the DEP starts to rise from 0 and eventually reaches a convergence value. This indicates that better channel conditions lead to an increased error detection probability for the warden, thereby making detection more challenging. Furthermore, once $\overline{\gamma}$ reaches a certain level, it no longer significantly affects the DEP. Additionally, larger values of

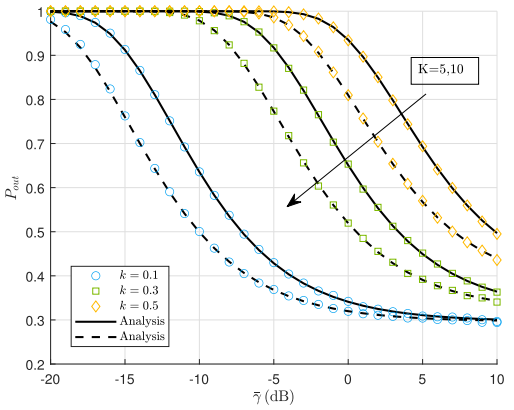

Fig. 5. P_{out} versus $\bar{\gamma}$ under different k and K with $N = 3$, $\bar{\gamma}_I = -10$dB, $P_{total} = 10$dB.

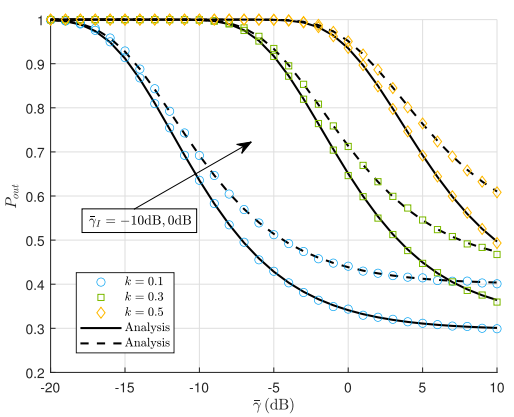

Fig. 6. P_{out} versus $\bar{\gamma}$ under different k and $\bar{\gamma}_I$ with $N = 3$, $P_{total} = 10$dB.

K result in higher DEP, as K represents the length of the estimation symbols, which means that a more accurate CSI increases the warden's detection difficulty.

Fig. 5 examines the OP via different $\overline{\gamma}$, different k, and different K. It is evident that the OP decreases monotonically with increasing $\overline{\gamma}$ for all parameter settings, reflecting the inherent improvement in link reliability at higher SNR regimes. For a fixed K, increasing the HIs level k leads to a pronounced rightward shift of the OP curves, indicating performance degradation. This behavior stems from the fact that a larger k represents more severe hardware impairments, which introduce additional distortion noise, thereby reducing the effective signal quality and increasing the likelihood of outage. Conversely, for a fixed k, increasing K yields a leftward shift of the OP curves, implying improved outage performance.

Fig. 6 derives the OP via different $\overline{\gamma}$, different $\overline{\gamma}_I$, and different k with $N = 3$, $P_{total} = 10$dB. As observed, for all curves corresponding to different k values, OP monotonically decreases with the increase of $\bar{\gamma}$. This trend shows that a higher $\overline{\gamma}$ can effectively reduce the likelihood of communication outages. Regarding the impact of HIs level k, it is evident that a larger k results in a higher OP at the same $\overline{\gamma}$. For instance, comparing the curves of $k = 0.5$ and $k = 0.1$, the former exhibits a notably higher outage probability, which demonstrates that severe hardware impairments can degrade signal

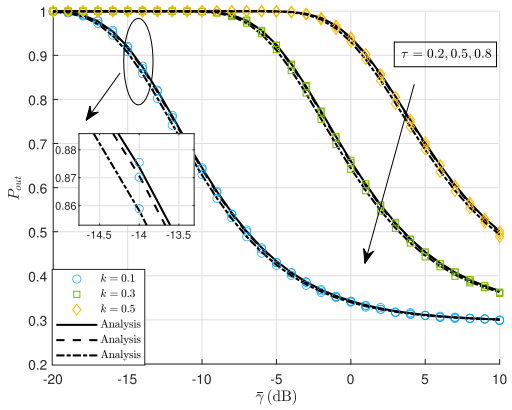

Fig. 7. P_{out} versus $\bar{\gamma}$ under different k and τ with $N = 3$, $\bar{\gamma}_I = -10$dB, $P_{total} = 10$dB.

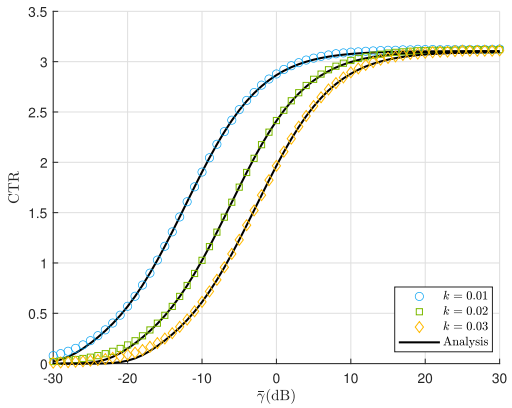

Fig. 8. CTR versus $\bar{\gamma}$ under different k with $N = 3$, $\bar{\gamma}_I = 15$dB, $P_{total} = 30$dB.

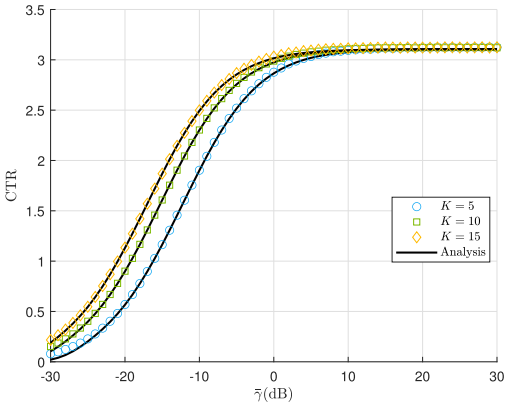

Fig. 9. CTR versus $\bar{\gamma}$ under different K with $N = 3$, $\bar{\gamma}_I = 15$dB, $P_{total} = 30$dB.

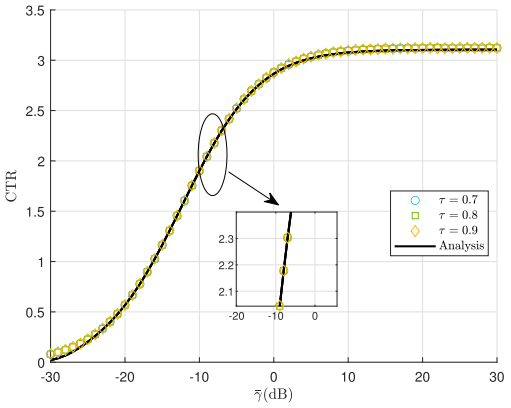

Fig. 10. CTR versus $\bar{\gamma}$ under different τ with $N = 3$, $\bar{\gamma}_I = 15$dB, $P_{total} = 30$dB.

quality and elevate outage risks. Additionally, the influence of interference $\overline{\gamma}_I$ is also distinguishable. As indicated by the annotation and the corresponding curve variations, stronger interference leads to an increase in OP. This is because intense interference can suppress the desired signal, thereby deteriorating the communication quality.

Fig. 7 depicts the OP via different $\overline{\gamma}$, different k, and different τ with $N = 3$, $\bar{\gamma}_I = -10$dB, $P_{total} = 10$dB. As $\overline{\gamma}$ increases, the OP gradually decreases due to the improvement in channel conditions, which reduces the likelihood of communication interruptions. A larger k leads to a higher OP, as the increased HIs level causes signal distortion and higher CEE, thereby reducing system reliability and increasing OP. Furthermore, the impact of varying τ values on OP is relatively insignificant.

Fig. 8 introduces the CTR via different $\overline{\gamma}$ and different k. From the figure, it can be observed that the CTR increases with the rise of $\overline{\gamma}$, eventually converging to an upper limit. This is due to improved channel conditions, which enhance the system's communication rate limit. Furthermore, the value of k has a significant impact on CTR. As k increases, CTR curve shifts to the right, which is attributed to the increase in the HIs level, leading to a reduction in CTR. Additionally, the upper convergence limit of CTR remains largely consistent across different k values.

Fig. 9 shows the CTR via different $\overline{\gamma}$ and different K with $N = 3$, $\bar{\gamma}_I = 15$dB, $P_{total} = 30$dB. In this figure, the variation trend of CTR with respect to $\overline{\gamma}$ follows a similar pattern as in the previous figure, with an upper rate limit still observed. Notably, larger values of K result in higher CTR, which can be attributed to more accurate CSI, highlighting the importance of channel estimation.

Fig. 10 examines the CTR via different $\overline{\gamma}$ and different τ with $N = 3$, $\bar{\gamma}_I = 15$dB, $P_{total} = 30$dB. It is evident that the impact of different τ values on CTR is minimal. This indicates that the power allocation has a negligible effect on the covert transmission performance of the system in terms of CTR, suggesting that adjusting the power allocation factor τ does not lead to a significant improvement in the CTR of the considered system.

V. Conclusion

In this paper, the covert transaction for the CISAGNs with a relay and two NOMA users was investigated. To improve the covert performance, spectrum efficiency, and resource utilization of the considered system, NOMA and cognitive technology were used. Additionally, practical challenges such as imperfect hardware, imperfect channel estimation, and co-channel interferences were also considered, reflecting the real-world network conditions. To reduce system complexity, a partial UAV selection scheme is introduced, optimizing the

operational efficiency of the network. Based on the above discussions, the closed-form expressions of DEP, OP, and CTR were derived. Extensive Monte Carlo simulation results validated the correctness of our theoretical derivations. Based on the above analysis, it is evident that CEE, HIs, cognitive technology, and NOMA significantly influenced the system's covert performance evaluation to varying extents. Besides, the derived upper bounds on the CTR can provide valuable insights for the design of low-power stealthy communication networks, particularly in military or emergency scenarios, where minimizing detectability while maintaining efficient communication is critical. Future extensions could further enhance the practicality of the framework. For instance, integrating machine learning-based power control could enable adaptive adjustment of transmission parameters in dynamic environments, optimizing covertness and efficiency in real time. Additionally, exploring dynamic warden mobility models would better reflect real-world adversarial behaviors, leading to more robust covert communication strategies against unpredictable detection threats.

Appendix A
Proof of Theorem 1

When recalling (37) and (38), it is obvious that the expressions on both sides can be easily derived, so we only focus on the expression in the middle part. Therefore, (37) can be rewritten as

$$\Pr\left(D_1|H_0\right)=\Pr\left(\lambda_{CW}\left(1+k_C^2\right)+1\geq\gamma_0\right)=1-e^{-\frac{\gamma_0-1}{1+k_C^2}}, \tag{59}$$

by taking (23) into (59), (37) will be obtained. The focusing next step is the derivation of (38).

$$\begin{aligned}\Pr\left(D_0|H_1\right)&=\Pr\left(\lambda_{CW}\leq\frac{T_6+T_5\lambda_{RP}-T_3\lambda_{RW}}{T_2\lambda_{RP}+T_4}\right)\\&=\int_a^{\infty}f_{\lambda_{RP}}\left(z\right)\left(H_1-H_2+H_3\right)dz,\end{aligned} \tag{60}$$

where $a=\max\left(0,-\frac{T_6}{T_5}\right)$, $H_1=1-\exp\left(-\frac{T_5z+T_6}{T_3\overline{\lambda}_{RW}}\right)$, $H_2=\frac{\overline{\lambda}_{CW}(T_2z+T_4)}{\overline{\lambda}_{CW}(T_2z+T_4)-\overline{\lambda}_{RW}T_3}\exp\left(-\frac{T_5z+T_6}{\overline{\lambda}_{CW}(T_2z+T_4)}\right)$, $H_3=\frac{\overline{\lambda}_{CW}(T_2z+T_4)}{\overline{\lambda}_{CW}(T_2z+T_4)-\overline{\lambda}_{RW}T_3}\exp\left(-\frac{T_5z+T_6}{\overline{\lambda}_{RW}T_3}\right)$.

Due to the uncertainty of the sign of the lower limit of the integral, we segment the function based on the sign of T_6, that is, (39), (40), (41), and (53)–(55), as shown at the bottom of the page 9. Then by substituting (25) into the above respective expressions, P_{MD} will be derived.

Appendix B
Proof of Theorem 2

Reviewing (44), it is essential to obtain the closed-form expressions for the probabilities of each component before deriving the OP. Taking $\Pr\left(\gamma_{D_1}\leq\gamma_0\right)$ as an example, the first part of (45) can be rewritten as

$$\begin{aligned}P_2\left(\gamma_0\right)=&\Pr\left(\gamma_{D_2,D_1}\leq\gamma_0\right)+\Pr\left(\gamma_{D_1,D_1}\leq\gamma_0\right)\\&-\Pr\left(\gamma_{D_2,D_1}\leq\gamma_0\right)\Pr\left(\gamma_{D_1,D_1}\leq\gamma_0\right),\end{aligned} \tag{61}$$

and

$$\begin{aligned}&\Pr\left(\gamma_{D_1,D_1}\leq\gamma_0\right)\\&=\Pr\left(\frac{\lambda_{RD_1}}{\lambda_{RD_1}\Theta_1+\lambda_{RP}\Psi_3+\lambda_{RP}\lambda_{ID_1}\mathrm{K}_3+\mathrm{X}_3}\leq\gamma_0\right)\\&=\frac{(J_1-J_2)}{(N-1)!\overline{\lambda}_{RP}^N},\end{aligned} \tag{62}$$

where

$$J_1=\int_0^{\infty}z^{N-1}\exp\left(-\frac{z}{\overline{\lambda}_{RP}}\right)dz, \tag{63}$$

$$J_2=\int_0^{\infty}z^{N-1}\exp\left(-\frac{z}{\overline{\lambda}_{RP}}\right)\frac{\mathcal{T}\exp\left(-\frac{\gamma_0(\Psi_3z+\mathrm{X}_3)}{\mathcal{T}}\right)}{\mathcal{T}+\overline{\lambda}_{ID_1}\gamma_0\left(\Phi_3z+\mathrm{K}_3\right)}dz. \tag{64}$$

where $\mathcal{T}=\overline{\lambda}_{RD_1}\left(1-\Theta_3\gamma_0\right)$. Then by taking (63) and (64) into (62), we will get

$$\begin{aligned}\Pr\left(\gamma_{D_1,D_1}\leq\gamma_0\right)=1-&\frac{\overline{\lambda}_{RD_1}\left(1-\Theta_3\gamma_0\right)}{(N-1)!\left(\overline{\lambda}_{RP}\right)^N}\\&\times\frac{\exp\left[-\frac{\gamma_0\mathrm{X}_3}{\mathcal{T}}\right]}{\overline{\lambda}_{ID_1}\gamma_0\Phi_3}\times H\left(N-1,\mu_3,\beta_3\right),\end{aligned} \tag{65}$$

where $\mu_3=\frac{\mathcal{T}+\overline{\lambda}_{RP}\gamma_0\Psi_3}{\overline{\lambda}_{RP}\mathcal{T}_\infty}$,$\beta_3=\frac{\overline{\lambda}_{ID_1}\gamma_0\mathrm{K}_3+\mathcal{T}}{\overline{\lambda}_{ID_1}\gamma_0\Phi_3}$.

In a similar way,

$$\begin{aligned}&\Pr\left(\gamma_{D_2,D_1}\leq\gamma_0\right)\\&=\Pr\left(\frac{\lambda_{RD_2}}{\mathcal{U}}\leq\gamma_0\right)=\frac{(J_1-J_3)}{(N-1)!\overline{\lambda}_{RP}^N},\end{aligned} \tag{66}$$

where $\mathcal{U}=\lambda_{RD_2}\Theta_1+\lambda_{RP}\Psi_1+\lambda_{RP}\lambda_{ID_2}\Phi_1+\lambda_{ID_2}\mathrm{K}_1+\mathrm{X}_1$,

$$J_3=\int_0^{\infty}z^{N-1}\exp\left(-\frac{z}{\overline{\lambda}_{RP}}\right)\frac{\mathcal{I}\exp\left(-\frac{\gamma_0(\Psi_1z+\mathrm{X}_1)}{\mathcal{I}}\right)}{\mathcal{I}+\overline{\lambda}_{ID_2}\gamma_0\left(\Phi_1z+\mathrm{K}_1\right)}dz. \tag{67}$$

where $\mathcal{I}=\overline{\lambda}_{RD_2}\left(1-\Theta_1\gamma_0\right)$. Then by substituting (63) and (67) into (66), we will obtain

$$\begin{aligned}\Pr\left(\gamma_{D_2,D_1}\leq\gamma_0\right)=1-&\frac{\mathcal{I}}{(N-1)!\left(\overline{\lambda}_{RP}\right)^N}\\&\times\frac{\exp\left[-\frac{\gamma_0\mathrm{X}_1}{\mathcal{I}}\right]}{\overline{\lambda}_{ID_2}\gamma_0\Phi_1}\times H\left(N-1,\mu_1,\beta_1\right),\end{aligned} \tag{68}$$

where $\mu_1=\frac{\mathcal{I}+\overline{\lambda}_{RP}\Psi_1\gamma_0}{\overline{\lambda}_{RP}\mathcal{I}}$, $\beta_1=\frac{\overline{\lambda}_{ID_2}\gamma_0\mathrm{K}_1+\mathcal{I}}{\overline{\lambda}_{ID_2}\gamma_0\Phi_1}$, and $H\left(n,\mu,\beta\right)=(-1)^{n-1}\beta^ne^{\beta\mu}\mathrm{Ei}\left(-\beta\mu\right)+\sum_{\lambda=1}^{n}(\lambda-1)!(-\beta)^{n-\lambda}\mu^{-\lambda}$,

and

$$\begin{aligned}&\Pr\left(\gamma_{R,1}\leq\gamma_0\right)\\&=\Pr\left(\frac{\lambda_{SR}a_1^2}{\lambda_{SR}AA+\lambda_{SP}BB+CC}\leq\gamma_0\right)\end{aligned}$$

$$= 1 - \sum_{k_{SR}=0}^{\varsigma_{SR}-1} \sum_{q=0}^{k_{SR}} \int_0^{\infty} \frac{(1-\varsigma_{SR})_{k_{SR}} (-\phi_{SR})^{k_{SR}} \alpha_{SR}}{(k_{SR}!)^2 \Delta_{SR}^{k_{SR}-q+1} \overline{\lambda}_{SR}^{k_{SR}}} \times \left[\frac{\gamma_0 (BBy+CC)}{a_1^2 - AA\gamma_0}\right]^q \exp\left(-\frac{\Delta_{SR}\gamma_0 (BBy+CC)}{a_1^2 - AA\gamma_0}\right) \times f_{\lambda_{SP}}(y)\, dy. \quad (69)$$

Then by taking (33) into (69), (56) will be obtained.

Appendix C
Proof of Theorem 3

With the help of [61], (51) and (52) have the expressions as

$$\begin{aligned} R_{D_1} &= E\left[\log_2\left(1+\min\left(\gamma_{D_2,D_1}, \gamma_{D_1,D_1}\right)\right)\right] \\ &= \int_0^{\gamma_D^{\max}} \log_2(1+x)\, f_{\gamma_1}(x)\, dx \\ &= \log_2(1+x)\, dF_{\gamma_1}(x) \\ &= \log_2(1+x)\, F_{\gamma_1}(x)\,|_0^{\gamma_D^{\max}} - \int_0^{\gamma_D^{\max}} \frac{F_{\gamma_1}(x)}{\ln 2\,(1+x)} dx. \end{aligned} \quad (70)$$

$$\begin{aligned} R_{D_2} &= E\left[\log_2\left(1+\gamma_{D_2,D_2}\right)\right] \\ &= \int_0^{\gamma_D^{\max}} \log_2(1+x)\, f_{\gamma_{D_2,D_2}}(x)\, dx \\ &= \log_2(1+x)\, dF_{\gamma_{D_2,D_2}}(x) \\ &= \log_2(1+x)\, F_{\gamma_{D_2,D_2}}(x)\,|_0^{\gamma_D^{\max}} - \int_0^{\gamma_D^{\max}} \frac{F_{\gamma_{D_2,D_2}}(x)}{\ln 2\,(1+x)} dx. \end{aligned} \quad (71)$$

where $\gamma_1 = \min\left(\gamma_{D_2,D_1}, \gamma_{D_1,D_1}\right)$, $\gamma_D^{\max} = \min\left[\min\left(\frac{1}{\Theta_1}, \frac{1}{\Theta_3}\right), \frac{1}{\Theta_2}\right]$. Besides, it is not hard to find that $F_{\gamma_1}(x)$ and $F_{\gamma_{D_2,D_2}}(x)$ have the same expression as (61) and (47). Then by taking (68) and (65) into (70), (47) into (71), with the help of [62], (51) and (52) will be obtained. Finally, by inserting (51) into (52), the CTR of the considered system will be obtained. The proof is completed.

References

[1] R. Liu et al., "RIS-empowered satellite-aerial-terrestrial networks with PD-NOMA," *IEEE Commun. Surveys Tuts.*, vol. 26, no. 4, pp. 2258–2289, 4th Quart., 2024.

[2] W. Wang, D. Niyato, Z. Xiong, and Z. Yin, "AUTHFi: Cross-technology device authentication via commodity WiFi," *IEEE Trans. Mobile Comput.*, vol. 24, no. 8, pp. 6765–6779, Aug. 2025.

[3] O. Kodheli et al., "Satellite communications in the new space era: A survey and future challenges," *IEEE Commun. Surveys Tuts.*, vol. 23, no. 1, pp. 70–109, 1st Quart., 2021.

[4] X. Liu, K.-Y. Lam, F. Li, J. Zhao, L. Wang, and T. S. Durrani, "Spectrum sharing for 6G integrated satellite-terrestrial communication networks based on NOMA and CR," *IEEE Netw.*, vol. 35, no. 4, pp. 28–34, Jul. 2021.

[5] J. Du, H. Wang, C. Jiang, J. Simonjan, J. Wang, and M. Debbah, "Distributed AI-based secure communications in space-air-ground-sea integrated networks," *IEEE Commun. Mag.*, vol. 63, no. 7, pp. 48–55, Jul. 2025.

[6] Z. Lin, Z. Feng, K. Guo, A. Nauman, D. Niyato, and J. Wang, "AI-driven seamless and massive access in space-air-ground integrated networks," *IEEE Wireless Commun.*, vol. 32, no. 3, pp. 72–79, Jun. 2025.

[7] M. A. Jamshed et al., "A tutorial on non-terrestrial networks: Towards global and ubiquitous 6G connectivity," *Found. Trends Netw.*, vol. 14, no. 3, pp. 160–253, Feb. 2025.

[8] H. Zhang et al., "Trustworthiness evaluation toward 6G support of space-air-ground integrated network," *IEEE Wireless Commun.*, vol. 32, no. 2, pp. 34–40, Apr. 2025.

[9] G. Peng, S. Wang, G. Li, T. Huang, Y. Huang, and Y. Liu, "Space-terrestrial integrated time-sensitive networks: Architecture, challenges, and open issues," *IEEE Netw.*, vol. 39, no. 3, pp. 140–147, May 2025.

[10] Z. Guo, K. Yu, N. Kumar, W. Wei, S. Mumtaz, and M. Guizani, "Deep-distributed-learning-based POI recommendation under mobile-edge networks," *IEEE Internet Things J.*, vol. 10, no. 1, pp. 303–317, Jan. 2023.

[11] *Digital Video Broadcasting (DVB); System Specifications for Satellite Services to Handheld Devices (SH) Below 3 GHz*, document ETSI TS 102 585 V1.1.2, Apr. 2008.

[12] M. Wu, K. Guo, X. Li, A. Nauman, K. An, and J. Wang, "Optimization design in RIS-assisted integrated satellite-UAV-served 6G IoT: A deep reinforcement learning approach," *IEEE Internet Things Mag.*, vol. 7, no. 1, pp. 12–18, Jan. 2024.

[13] A. Khan et al., "Integrated non-terrestrial and terrestrial quantum anonymous networks," *IEEE Netw.*, vol. 39, no. 3, pp. 196–206, May 2025.

[14] M. R. Bhatnagar and A. Hjorungnes, "Differential coding for MAC based two-user MIMO communication systems," *IEEE Trans. Wireless Commun.*, vol. 11, no. 1, pp. 9–14, Jan. 2012.

[15] M. K. Arti, "Channel estimation and detection in hybrid satellite-terrestrial communication systems," *IEEE Trans. Veh. Technol.*, vol. 65, no. 7, pp. 5764–5771, Jul. 2016.

[16] Y. Zhang et al., "Energy-efficient resource allocation for satellite-UAV-ground integrated compute first networking," *IEEE Trans. Consum. Electron.*, early access, Sep. 17, 2025, doi: 10.1109/TCE.2025.3610868.

[17] P. K. Upadhyay and P. K. Sharma, "Max-max user-relay selection scheme in multiuser and multirelay hybrid satellite-terrestrial relay systems," *IEEE Commun. Lett.*, vol. 20, no. 2, pp. 268–271, Feb. 2016.

[18] K. Guo et al., "On the performance of the uplink satellite multiterrestrial relay networks with hardware impairments and interference," *IEEE Syst. J.*, vol. 13, no. 3, pp. 2297–2308, Sep. 2019.

[19] B. Zhao, M. Lin, S. Xiao, M. Cheng, J.-B. Wang, and J. Cheng, "Angular information based robust downlink transmission for IRS-enhanced cognitive satellite-aerial networks," *IEEE Trans. Veh. Technol.*, vol. 73, no. 1, pp. 559–575, Jan. 2024.

[20] Z. Lin, M. Lin, T. de Cola, J.-B. Wang, W.-P. Zhu, and J. Cheng, "Supporting IoT with rate-splitting multiple access in satellite and aerial-integrated networks," *IEEE Internet Things J.*, vol. 8, no. 14, pp. 11123–11134, Jul. 2021.

[21] X. Lin et al., "Secure beamforming and anti-jamming coalition formation for air-terrestrial integrated ad-hoc networks," *IEEE Trans. Wireless Commun.*, vol. 24, no. 8, pp. 6722–6736, Aug. 2025, doi: 10.1109/TWC.2025.3555600.

[22] M. Vaezi, R. Schober, Z. Ding, and H. V. Poor, "Non-orthogonal multiple access: Common myths and critical questions," *IEEE Wireless Commun.*, vol. 26, no. 5, pp. 174–180, Oct. 2019.

[23] K. An, M. Lin, W.-P. Zhu, Y. Huang, and G. Zheng, "Outage performance of cognitive hybrid satellite-terrestrial networks with interference constraint," *IEEE Trans. Veh. Technol.*, vol. 65, no. 11, pp. 9397–9404, Nov. 2016.

[24] K. An, M. Lin, J. Ouyang, and W.-P. Zhu, "Secure transmission in cognitive satellite terrestrial networks," *IEEE J. Sel. Areas Commun.*, vol. 34, no. 11, pp. 3025–3037, Nov. 2016.

[25] Z. Lin, M. Lin, B. Champagne, W.-P. Zhu, and N. Al-Dhahir, "Secure beamforming for cognitive satellite terrestrial networks with unknown eavesdroppers," *IEEE Syst. J.*, vol. 15, no. 2, pp. 2186–2189, Jun. 2021.

[26] Y. Ruan, L. Jiang, Y. Li, and R. Zhang, "Energy-efficient power control for cognitive satellite-terrestrial networks with outdated CSI," *IEEE Syst. J.*, vol. 15, no. 1, pp. 1329–1332, Mar. 2021.

[27] J. Ouyang, J. Ding, R. Wang, B. Zhao, and M. Lin, "Robust secrecy-energy efficient beamforming for jittering UAV in cognitive satellite-aerial networks," *IEEE Trans. Aerosp. Electron. Syst.*, vol. 61, no. 4, pp. 9567–9583, Aug. 2025.

[28] Z. Ding, X. Lei, G. K. Karagiannidis, R. Schober, J. Yuan, and V. K. Bhargava, "A survey on non-orthogonal multiple access for 5G networks: Research challenges and future trends," *IEEE J. Sel. Areas Commun.*, vol. 35, no. 10, pp. 2181–2195, Oct. 2017.

[29] W. Luo et al., "Outage evaluation for STAR-RIS-assisted satellite-AAV-terrestrial NOMA networks with imperfect CSI," *IEEE Internet Things J.*, vol. 12, no. 12, pp. 19981–19994, Jun. 2025.

[30] J. Li et al., "Active RIS-aided NOMA-enabled space-air-ground integrated networks with cognitive radio," *IEEE J. Sel. Areas Commun.*, vol. 43, no. 1, pp. 314–333, Jan. 2025.

[31] X. Wang, H. Chen, and F. Tan, "Hybrid OMA/NOMA mode selection and resource allocation in space-air-ground integrated networks," *IEEE Trans. Veh. Technol.*, vol. 74, no. 1, pp. 699–713, Jan. 2025.

[32] G. Xu, Z. Zhao, Z. Song, Q. Zhang, and B. Ai, "Symbol error analysis for integrated satellite- terrestrial relay networks with non-orthogonal multiple access under hardware impairments," *IEEE Trans. Wireless Commun.*, vol. 23, no. 10, pp. 12980–12994, Oct. 2024.

[33] Y. Omid et al., "Reinforcement learning-based downlink transmit precoding for mitigating the impact of delayed CSI in satellite systems," *IEEE Trans. Commun.*, early access, May 13, 2025, doi: 10.1109/TCOMM.2025.3569690.

[34] F. Zhou, R. Wang, and K. Guo, "Secrecy outage analysis of satellite communication networks with hardware impairments and channel estimation errors," *Electron. Lett.*, vol. 56, no. 20, pp. 1059–1062, Sep. 2020.

[35] K. Guo, C. Dong, and K. An, "NOMA-based cognitive satellite terrestrial relay network: Secrecy performance under channel estimation errors and hardware impairments," *IEEE Internet Things J.*, vol. 9, no. 18, pp. 17334–17347, Sep. 2022.

[36] Z. Yin et al., "Multi-domain resource multiplexing based secure transmission for satellite-assisted IoT: AO-SCA approach," *IEEE Trans. Wireless Commun.*, vol. 22, no. 11, pp. 7319–7330, Nov. 2023.

[37] W. Wang et al., "Secure enhanced IoT-WLAN authentication protocol with efficient fast reconnection," *IEEE Trans. Mobile Comput.*, vol. 24, no. 10, pp. 10085–10098, Oct. 2025.

[38] Z. Yin, N. Cheng, T. H. Luan, and P. Wang, "Physical layer security in cybertwin-enabled integrated satellite-terrestrial vehicle networks," *IEEE Trans. Veh. Technol.*, vol. 71, no. 5, pp. 4561–4572, May 2022.

[39] B. Li, Z. Fei, C. Zhou, and Y. Zhang, "Physical-layer security in space information networks: A survey," *IEEE Internet Things J.*, vol. 7, no. 1, pp. 33–52, Jan. 2020.

[40] K. Guo et al., "Physical layer security for multiuser satellite communication systems with threshold-based scheduling scheme," *IEEE Trans. Veh. Technol.*, vol. 69, no. 5, pp. 5129–5141, May 2020.

[41] M. Ji, M. Lin, Z. Wang, J. Ouyang, and N. Al-Dhahir, "Queue-stability constrained robust secure beamforming in satellite-terrestrial integrated networks," *IEEE Commun. Lett.*, vol. 29, no. 5, pp. 1032–1036, May 2025.

[42] M. Huang et al., "Robust secure precoding for UAV-aided multi-beam satellite NOMA communications," *IEEE Trans. Veh. Technol.*, vol. 73, no. 6, pp. 8069–8082, Jun. 2024.

[43] J. Zhang, J. Wang, X. Li, S. Li, Z. Yuan, and G. Pan, "Secrecy analysis for NOMA-based multi-antenna satellite-UAV-terrestrial SWIPT systems," *IEEE Trans. Green Commun. Netw.*, vol. 8, no. 2, pp. 672–685, Jun. 2024.

[44] C. Han, A. Liu, Z. Gao, K. An, G. Zheng, and S. Chatzinotas, "Anti-jamming transmission in NOMA-based satellite-enabled IoT: A game-theoretic framework in hostile environments," *IEEE Internet Things J.*, vol. 10, no. 23, pp. 20311–20322, Dec. 2023.

[45] Z. Ding et al., "A state-of-the-art survey on reconfigurable intelligent surface-assisted non-orthogonal multiple access networks," *Proc. IEEE*, vol. 110, no. 9, pp. 1358–1379, Sep. 2022.

[46] X. Jiang et al., "Covert communication in UAV-assisted air-ground networks," *IEEE Wireless Commun.*, vol. 28, no. 4, pp. 190–197, Aug. 2021.

[47] J. An, B. Kang, Q. Ouyang, J. Pan, and N. Ye, "Covert communications meet 6G NTN: A comprehensive enabler for safety-critical IoT," *IEEE Netw.*, vol. 38, no. 4, pp. 17–24, Jul. 2024.

[48] K. Guo et al., "Covert communications for energy-efficient ISTRNs with opportunistic scheduling and cooperative jamming," *IEEE Trans. Green Commun. Net.*, early access, Mar. 11, 2025, doi: 10.1109/TGCN.2025.3550262.

[49] S. Feng, X. Lu, S. Sun, E. Hossain, G. Wei, and Z. Ni, "Covert communication in large-scale multi-tier LEO satellite networks," *IEEE Trans. Mobile Comput.*, vol. 23, no. 12, pp. 11576–11587, Dec. 2024.

[50] D. Song, Z. Yang, G. Pan, S. Wang, and J. An, "RIS-assisted covert transmission in satellite-terrestrial communication systems," *IEEE Internet Things J.*, vol. 10, no. 22, pp. 19415–19426, Nov. 2023.

[51] H. Peng et al., "Ambient backscatter communication symbiotic intelligent transportation systems: Covertness performance analysis and optimization," *IEEE Trans. Consum. Electron.*, vol. 70, no. 1, pp. 1833–1844, Feb. 2024.

[52] E. Costa and S. Pupolin, "M-QAM-OFDM system performance in the presence of a nonlinear amplifier and phase noise," *IEEE Trans. Commun.*, vol. 50, no. 3, pp. 462–472, Mar. 2002.

[53] T. Schenk, *RF Imperfections in High-rate Wireless Systems: Impact and Digital Compensation*. Cham, Switzerland: Springer, 2008, pp. 2033–2043.

[54] C. Studer, M. Wenk, and A. Burg, "MIMO transmission with residual transmit-RF impairments," in *Proc. Int. ITG Workshop Smart Antennas (WSA)*, Tennenlohe, Germany, Feb. 2010, pp. 189–196.

[55] E. Bjornson, M. Matthaiou, and M. Debbah, "A new look at dual-hop relaying: Performance limits with hardware impairments," *IEEE Trans. Commun.*, vol. 61, no. 11, pp. 4512–4525, Nov. 2013.

[56] K. Guo, M. Lin, B. Zhang, W.-P. Zhu, J.-B. Wang, and T. A. Tsiftsis, "On the performance of LMS communication with hardware impairments and interference," *IEEE Trans. Commun.*, vol. 67, no. 2, pp. 1490–1505, Feb. 2019.

[57] G. Xu, Y. Zhu, L. Wang, Y. Wang, and B. Shen, "Ergodic capacity of a NOMA-based RF/FSO integrated satellite-terrestrial relay networks system," *IEEE Photon. Technol. Lett.*, vol. 37, no. 11, pp. 621–624, Jun. 1, 2025.

[58] M. Asif et al., "Transmissive RIS-empowered LEO-satellite communications with hybrid-NOMA under residual hardware impairments," *IEEE Trans. Green Commun. Net.*, vol. 9, no. 3, pp. 1167–1178, Sep. 2024, doi: 10.1109/TGCN.2024.3466469.

[59] F. Zhou et al., "Performance evaluations for RIS-aided satellite aerial terrestrial integrated networks with link selection scheme and practical limitations," *IEEE Trans. Netw. Service Manage.*, vol. 22, no. 4, pp. 3179–3190, Aug. 2025.

[60] P. Qi et al., "Reliable covert communication in NOMA-aided cognitive satellite aerial terrestrial integrated networks," *IEEE Internet Things J.*, early access, Aug. 25, 2025, doi: 10.1109/JIOT.2025.3602642.

[61] Y. Zhang, L. Yang, X. Li, K. Guo, and H. Liu, "Covert communications for STAR-RIS-assisted industrial networks with a full duplex receiver and RSMA," *IEEE Internet Things J.*, vol. 11, no. 12, pp. 22483–22493, Jun. 2024.

[62] M. Abramowitz and I. A. Stegun, *Handbook of Mathematical Functions With Formulas, Graphs, and Mathematical Tables*, 9th ed., New York, NY, USA: Dover, 1972.

[63] I. S. Gradshteyn, *Table of Integrals, Series and Products*, 7th ed., Amsterdam, The Netherlands: Elsevier, 2007.

Liuying Zhou was born in Jiujiang, Jiangxi, China. She received the M.S. degree from Soochow University, Suzhou, China, in 2011. She has been a Lecturer with the School of Foreign Language, Yancheng Institute of Technology, Yancheng, China. Her research interests include satellite communication and covert communication.

Peilin Qi (Graduate Student Member, IEEE) received the B.S. degree from Army Engineering University, Nanjing, China, in 2023. She is currently pursuing the M.S. degree with the College of Electronic and Information Engineering, Nanjing University of Aeronautics and Astronautics, Nanjing, China. Her current research interests include satellite communication, NOMA technology, and covert communication.

Kefeng Guo received the B.S. degree from Beijing Institute of Technology, Beijing, China, in 2012, and the Ph.D. degree from Army Engineering University, Nanjing, China, in 2018. He is currently an Associate Professor with the College of Electronic and Information Engineering, Nanjing University of Aeronautics and Astronautics. He was listed in the World's Top 2% Scientists identified by Stanford University in 2022–2025. He has authored or co-authored nearly 100 research papers in international journals and conferences. His research interests include cooperative relay networks, MIMO communications systems, multiuser communication systems, satellite communication, hardware impairments, cognitive radio, NOMA technology, and physical layer security. He has been a TPC member of many IEEE sponsored conferences, such as IEEE ICC, IEEE GLOBECOM, and IEEE WCNC. He was a recipient of the Exemplary Reviewer for IEEE TRANSACTIONS ON COMMUNICATIONS in 2022. He was the recipient of the Outstanding Ph.D. Thesis Award of Chinese Institute of Command and Control in 2020. He was the recipient of the Best Paper Award of WiSATS 2024 and NCIC 2024. He was also the recipient of the Excellent Ph.D. Thesis Award of Jiangsu Province, China, in 2020. He also serves as an Editor on the Editorial Board for the *EURASIP Journal on Wireless Communications and Networking* and IEEE OPEN JOURNAL OF THE COMMUNICATIONS SOCIETY.

Ali Nauman received the Ph.D. degree in information and communication engineering from Yeungnam University, Gyeongsan, Republic of Korea, in 2022. He is the Founder of IEEE ComSoc Special Interest Group on AI for Integrated TN and NTN (AITNTN). He is currently an Assistant Professor with the Department of Computer Science and Engineering, Yeungnam University. He has contributed to five patents and authored/co-authored five book chapters and more than 100 technical papers in leading journals and peer-reviewed conferences. The main domain of his research is in the field of artificial intelligence-enabled wireless networks for non-terrestrial networks, tactile healthcare, multimedia, and Industry 5.0. His research interest includes resource allocation for 5G and Beyond-5G (B5G) networks, device-to-device communication (D2D)/V2X, Internet of Everything (IoE), and URLLC. He has also edited two books and serves as an editor and a reviewer of highly reputed journals and conferences.

Lei Zhang received the B.E. and M.S. degrees from Nanjing Institute of Communication Engineering, Nanjing, China, in 1994 and 1997, respectively, and the Ph.D. degree from PLA University of Science and Technology, Nanjing, in 2000.

From 2001 to 2003, he was a Post-Doctoral Researcher with Southeast University, Nanjing. He is currently a Professor with the College of Electronic and Information Engineering, Nanjing University of Aeronautics and Astronautics, Nanjing. His research interests include edge computing, embedded systems, CPS, and wireless ad-hoc networks.

Qihui Wu received the B.S. degree in communications engineering and the M.S. and Ph.D. degrees in communications and information systems from the Institute of Communications Engineering, Nanjing, China, in 1994, 1997, and 2000, respectively. From 2003 to 2005, he was a Post-Doctoral Research Associate with Southeast University, Nanjing. From 2005 to 2007, he was an Associate Professor with the College of Communications Engineering, PLA University of Science and Technology, Nanjing, where he was a Full Professor, from 2008 to 2016. From March 2011 to September 2011, he was an Advanced Visiting Scholar with the Stevens Institute of Technology, Hoboken, NJ, USA. Since May 2016, he has been a Full Professor with the College of Electronic and Information Engineering, Nanjing University of Aeronautics and Astronautics, Nanjing. His current research interests include the areas of wireless communications and statistical signal processing, with emphasis on system design of software defined radio, cognitive radio, and smart radio.

Sung Won Kim received the B.S. and M.S. degrees from the Department of Control and Instrumentation Engineering, Seoul National University, South Korea, in 1990 and 1992, respectively, and the Ph.D. degree from the School of Electrical Engineering and Computer Sciences, Seoul National University, in August 2002. From January 1992 to August 2001, he was a Researcher with the Research and Development Center of LG Electronics, South Korea. From August 2001 to August 2003, he was a Researcher with the Research and Development Center of AL Tech, South Korea. From August 2003 to February 2005, he was a Post-Doctoral Researcher with the Department of Electrical and Computer Engineering, University of Florida, Gainesville, FL, USA. In March 2005, he joined the Department of Information and Communication Engineering, Yeungnam University, Gyeongsangbuk-do, South Korea, where he is currently a Professor. His research interests include resource management, wireless networks, mobile computing, performance evaluation, and machine learning.